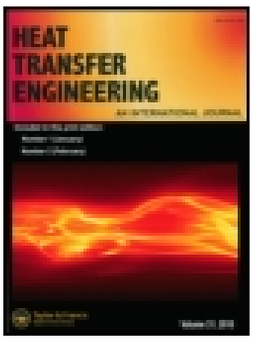

Heat Transfer Engineering

ISSN: 0145-7632 (Print) 1521-0537 (Online) Journal homepage: http://www.tandfonline.com/loi/uhte20

One-Phase and Two-Phase Flow in Highly Permeable Porous Media

Yohan Davit & Michel Quintard

To cite this article: Yohan Davit & Michel Quintard (2018): One-Phase and Two-Phase Flow in Highly Permeable Porous Media, Heat Transfer Engineering, DOI: 10.1080/01457632.2018.1432018

To link to this article: https://doi.org/10.1080/01457632.2018.1432018

Accepted author version posted online: 25 Jan 2018.
Published online: 26 Feb 2018.

HEAT TRANSFER ENGINEERING
2018, VOL. 0, NO. 0, 1–19
https://doi.org/10.1080/01457632.2018.1432018

Taylor & Francis
Taylor & Francis Group

One-Phase and Two-Phase Flow in Highly Permeable Porous Media

Yohan Davit and Michel Quintard

Institut de Mécanique des Fluides de Toulouse (IMFT) - Université de Toulouse, CNRS-INPT-UPS, Toulouse, France

ABSTRACT

Many industrial and natural processes involve flow in highly permeable media, such as exchangers, canopies, urban canyons. Traditional assumptions used for modeling flow equations in low permeability structures may not hold for these systems with very large pores. Reynolds numbers may be too large so that Darcy's law is no longer valid. Large Capillary and Bond numbers may also invalidate the quasistatic assumptions implicit in many empirical formulations and upscaling results. In this paper, we review several approaches developed to handle such cases, basing our analysis on new experimental data and results from upscaling methods. For one-phase flow this has led to various formulations of macro-scale momentum transport including generalized Forchheimer equations and macro-scale turbulent models. For two-phase flows, we discuss possible ways toward deriving macro-scale models from the pore-scale equations and introduce several macro-scale models: generalized Darcy's laws, models with cross terms accounting for the viscous interaction between the flowing phases, formulations capturing inertial, or dynamic effects. Models suitable for describing flow in structured media like chemical exchangers containing structured packings are also introduced. Finally, we present hybrid representations that couple approaches at two different scales, for instance, a meso-scale network approach coupled with dynamic rules obtained from pore-scale numerical simulations or experiments. This approach proved useful in describing the diffusion of impinging jets in packed beds, which is not described properly by capillary diffusion.

Introduction

Current trends in porous media physics involve research on transport in structures with pores at both extremes of the size spectrum. One extreme corresponds to small pore sizes and very low permeabilities, such as oil-shales or nanoporous materials. The other extreme, which is the topic of this review, corresponds to highly permeable media with a pore size that can be much larger than the capillary lengths of the fluids. This is the case for many porous media used in chemical engineering, such as trickle beds—particles larger than the millimeter—or structured packings—pore size of about 1 cm. Other examples include fractured materials or geophysical formations, very coarse sands, natural and man-made canopies, nuclear reactors as well as debris beds in damaged nuclear cores. Although highly permeable porous media are of interest in many different fields, they have been given much less emphasis than low and medium permeability media.

In classical applications, macro-scale models are developed using a series of assumptions about the order of magnitudes of the relevant dimensionless numbers. For instance, one-phase flow are mostly considered in the limit where the Reynolds number (Re) goes to zero, this leading to the classical Darcy's law [1]. In the case of two-phase flow in porous media, Reynolds (Re), Bond (Bo), and capillary (Ca) numbers are often assumed to be small. This assumption is central to the validity of the so-called generalized Darcy's laws as introduced by [2].

Can we modify the macro-scale models to describe situations where one or all of these dimensionless numbers become very large? This problem has been the subject of intensive research in the past decades. Here, we review this work and discuss multiple aspects of the multiscale problems associated with one- and two-phase flow in highly permeable porous media. We put the emphasis on the structure of macro-scale models that have been developed and do not present other important issues, such as numerical modeling or experimental techniques that are specific to the highly permeable case.

CONTACT Dr. Michel Quintard michel.quintard@imft.fr Institut de Mécanique des Fluides de Toulouse (IMFT) - Université de Toulouse, CNRS-INPT-UPS, Toulouse 31000, France.

Color versions of one or more of the figures in this paper can be found online at www.tandfonline.com/uhte.

Definitions, hypotheses, and upscaling techniques

A variety of approaches have been proposed in the literature to obtain macro-scale representations directly from the pore-scale problem. One may look at [3]–[6] for a comparison between the various techniques. A representative sample of papers includes, among hundreds of relevant papers, the following works: [7]–[11] for volume averaging, [12]–[14] for homogenization theory, and [15]–[17] for stochastic approaches. In general, these methods apply to discretely hierarchical porous media and assume the existence of a representative elementary volume of characteristic length r_0. Many conditions must be fulfilled in order to obtain well-behaved average quantities, in particular smooth and differentiable fields in which high-frequency fluctuations have been filtered out. One fundamental condition is the separation of length scales, which is often written as

$$l_p, l_\sigma \ll r_0 \ll L, \tag{1}$$

where l_p and l_σ are pore-scale characteristic lengths and L is the length of the macroscopic domain (see Figure 1). Here, the subscript p in l_p refers to the pore-space, which can be filled with either one or two fluid phases. The inequalities Eq. (1) are essentially geometrical constraints, which is only an order of magnitude estimate. In a more precise presentation, the length-scales characterize the variation of physical variables, such as pressure and velocity fields, not of geometrical features of the porous structure. For instance, L is often associated with the characteristic length of spatially averaged quantities and the validity of the hypothesis of separation of scales is process and operator dependent. In the remainder of this paper, we assume that this assumption is valid for the different configurations and flow regimes. In addition to the separation of scales, there are also other conditions that are more specific to the type of averaging that is performed. For spatial averaging, for example, well-behaved averaged fields are obtained through spatial convolutions and multiple averaging techniques, see more details in [18]–[23]. This is beyond the scope of this review to provide the background about all these upscaling methods.

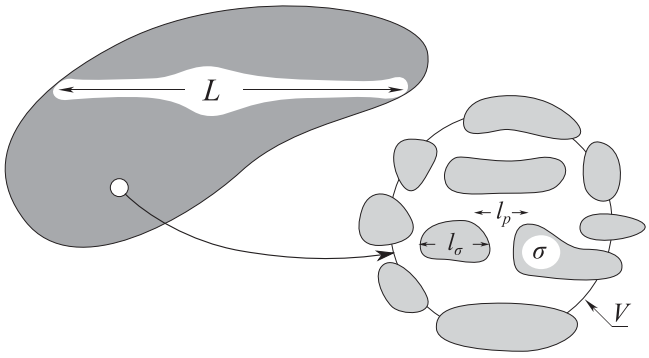

Figure 1. Schematic representation of a porous medium.

Here, the emphasis is on results specific to the case of highly permeable media, with references to the relevant literature on upscaling. In order to clarify the physical nature of the macro-scale fields introduced in the various models, we use the vocabulary and definitions of the volume averaging technique. We define the total and superficial spatial averages using the most simple mathematical apparatus (see the cited literature for a more thorough discussion and more general definitions using convolutions),

$$\langle \psi_\beta \rangle = \frac{1}{V} \int_{\mathcal{V}_\beta} \psi_\beta dV, \tag{2}$$

where $\mathcal{V}_\beta$ is the volume of the β-phase contained within V, the averaging volume represented in Figure 1, and ψ_β is a physical variable associated with the β-phase (e.g., pressure or concentration). The average of the β-phase indicator (a field having the value 1 in the β-phase, 0 elsewhere), denoted γ_β, yields

$$\varepsilon_\beta = \langle \gamma_\beta \rangle = \frac{1}{V} \int_{\mathcal{V}_\beta} dV = \frac{\mathcal{V}_\beta}{V}, \tag{3}$$

where ε_β is the β-phase volume fraction (porosity if this is the only phase in the pore-space). This can be used to define the intrinsic phase average, $\langle \psi_\beta \rangle^\beta$ as

$$\langle \psi_\beta \rangle = \varepsilon_\beta \langle \psi_\beta \rangle^\beta. \tag{4}$$

Finally, the porosity, ε, is defined as

$$\varepsilon = 1 - \varepsilon_\sigma \tag{5}$$

and the saturation of the β-phase, S_β, by

$$\varepsilon_\beta = \varepsilon S_\beta \tag{6}$$

with $S_\beta \in [0, 1]$.

One-phase flow

Let us consider the flow of a fluid (β-phase) within a porous structure (solid phase σ) with the fluid filling the entire pore space. The pore-scale problem describing the flow may be written for a Newtonian fluid with constant density, ρ_β, and viscosity, μ_β, as

$$\nabla \cdot \mathbf{v}_\beta = 0 \text{ in } \mathcal{V}_\beta \tag{7}$$

$$\rho_\beta \frac{\partial \mathbf{v}_\beta}{\partial t} + \rho_\beta \mathbf{v}_\beta \cdot \nabla \mathbf{v}_\beta = -\nabla p_\beta + \rho_\beta \mathbf{g} + \mu_\beta \nabla^2 \mathbf{v}_\beta \text{ in } \mathcal{V}_\beta \tag{8}$$

$$\text{B.C.1} \qquad \mathbf{v}_\beta = 0 \quad \text{at } A_{\beta\sigma}, \tag{9}$$

where $\mathbf{v}_\beta$ and p_β are the fluid velocity and pressure, respectively, g is the gravitational acceleration, and $A_{\beta\sigma}$

represents the interface between the fluid and solid phases.

The macro-scale variables needed for describing the flow of the β-phase are the intrinsic phase averaged pressure

$$P_\beta = \langle p_\beta \rangle^\beta \tag{10}$$

and the filtration velocity, $\mathbf{V}_\beta$, or intrinsic velocity, $\mathbf{U}_\beta$, defined as

$$\mathbf{V}_\beta = \langle \mathbf{v}_\beta \rangle = \varepsilon_\beta \langle \mathbf{v}_\beta \rangle^\beta = \varepsilon_\beta \mathbf{U}_\beta. \tag{11}$$

For one-phase flow of a Newtonian fluid, the important dimensionless parameter characterizing the flow is the pore-scale Reynolds number, which can be defined as

$$\mathrm{Re} = \frac{\rho_\beta U_r l_\beta}{\mu_\beta}, \tag{12}$$

where U_r is a reference velocity, often the intrinsic average velocity, and l_β a pore-scale characteristic length. We can use the Reynolds number to distinguish different flow regimes [24] corresponding to different macro-scale models.

Creeping flow

In the limit $\mathrm{Re} \to 0$ (creeping flow), there is a broad consensus for Darcy's law [1], provided that the separation of scales holds. This reads

$$\mathbf{V}_\beta = -\frac{1}{\mu_\beta}\mathbf{K} \cdot \left(\nabla P_\beta - \rho_\beta \mathbf{g}\right), \tag{13}$$

where $\mathbf{K}$ is the intrinsic permeability tensor. This equation, together with the macro-scale version of the mass balance equation,

$$\nabla \cdot \mathbf{V}_\beta = 0 \tag{14}$$

can be used to calculate the macro-scale velocity and pressure fields.

This macro-scale law is supported by many experimental results, in particular by Darcy's own experiments. It is also confirmed by theoretical developments. Upscaling Stokes equations at the pore-scale (Eqs. (7)–(9)) via homogenization theory [25] or volume averaging [20], [26] yields a sound physical basis for the use of Darcy's law. Key steps of the mathematical developments are as follows.

- Linearization of the Navier–Stokes equations in the limit $\mathrm{Re} \to 0$ to obtain Stokes' problem,
- Introduction of a coupled problem for macro-scale values and pore-scale deviations defined as

$$p_\beta = P_\beta + \tilde{p}_\beta \quad ; \quad \mathbf{v}_\beta = \mathbf{U}_\beta + \tilde{\mathbf{v}}_\beta \tag{15}$$

- Simplifications of the problem based on the separation of spatial scales,
- Introduction of an approximated solution of the coupled problem through a *closure*, which emerges from the mathematical structure of the Stokes problem. At first-order, this closure reads

$$\tilde{p}_\beta = \mu_\beta \, \mathbf{b} \cdot \mathbf{U}_\beta \, ; \tilde{\mathbf{v}} = \mathbf{B} \cdot \mathbf{U}_\beta, \tag{16}$$

where the vector $\mathbf{b}$ and tensor $\mathbf{B}$ are called mapping variables. These are solutions of a local problem that is usually solved over a representative unit cell (see the Appendix),

- Derivation of the macro-scale equation from the averaged equations and the closure: one obtains Darcy's law, Eq. (13) and the intrinsic permeability, given by

$$\mathbf{K}^{-1} = -\varepsilon_\beta^{-2} \frac{1}{V} \int_{A_{\beta\sigma}} \mathbf{n}_{\beta\sigma} \cdot (-\mathbf{I}\mathbf{b} + \nabla \mathbf{B}) \, dA, \tag{17}$$

which is calculated from the solution of the closure problem over the representative unit cell. Nowadays, this is almost a routine operation to calculate such effective properties from reconstructed 3D images, such as those obtained using X-ray microtomography.

Inertial effects for moderate Reynolds numbers

When the Reynolds number becomes sufficiently large, inertial effects start to predominate and the relation between the pressure drop and the average velocity becomes nonlinear. While the exact definition of the different regimes is still a matter of controversy [27]–[31], the apparent permeability that would reproduce the actual pressure–velocity relation may be roughly described as in Figure 2. The first nonlinear regime corresponds to a cubic dependence of the pressure drop upon the Reynolds number $\propto \mathrm{Re}^3$. This regime is often called the *weak inertial regime*, as inertial effects affect the drag but the flow is still laminar and steady. As the Reynolds number is increased beyond this regime, a *strong inertial regime* is usually observed that also corresponds to a steady flow but for which the pressure drop can be approximated as $\propto \mathrm{Re}^n$ with $1 \leq n \leq 2$. The exact value of n is difficult to evaluate. In the literature so far, n seems to depend upon the structure and order of the porous medium. For instance, the work in [31] indicates that the value of n is closer to 2 for disordered media than for order ones. Further, for some porous structures—maybe most of them—a single value of n cannot be defined [32] and the strong inertial regime seems to correspond to a transition regime. For even larger Reynolds numbers, a transition to unsteady flow occurs. When this happens, time fluctuations of the pressure and velocities must be considered. In this section, we limit our analysis to the onset of

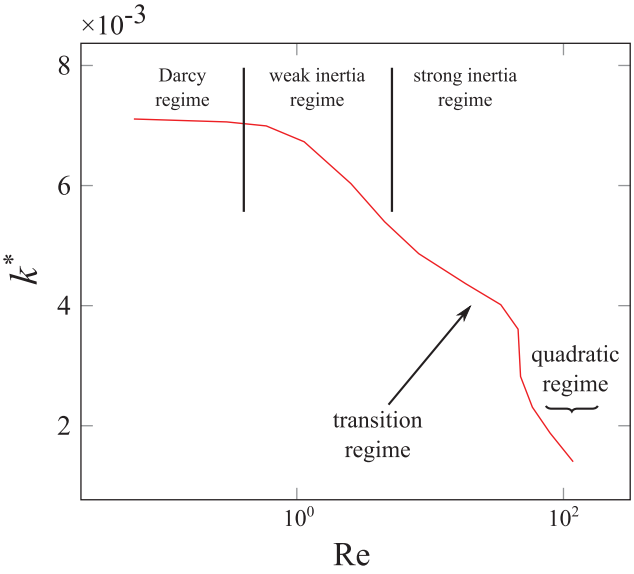

Figure 2. Various flow regimes characterized by the apparent permeability, k^*, as a function of the Reynolds number.

unsteady flows and small temporal fluctuations. We therefore neglect time fluctuations and concentrate on spatial averaging (we will see in Section Towards Turbulence in Porous Media how to deal with large temporal fluctuations.). Recent work in [32] suggests that the onset of unsteady flow corresponds to a quadratic regime and to a classical Forchheimer equation.

This has led to the proposal of heuristic laws having the form of a Forchheimer equation, which can be written in a very general manner as

$$0 = -\nabla P_\beta + \rho_\beta \mathbf{g} - \mu_\beta \mathbf{K}^{-1} \cdot \mathbf{V}_\beta - \mathbf{F}\left(\mathbf{V}_\beta\right) \cdot \mathbf{V}_\beta, \quad (18)$$

where the term $\mathbf{F}(\mathbf{V}_\beta) \cdot \mathbf{V}_\beta$ is called a generalized Forchheimer term in reference to the work in [33]. If one solves the upscaling problem using an asymptotic expansion in terms of Reynolds number, we can recover theoretically the first correction to Darcy's law, i.e., cubic terms in the weakly inertial regime [27]–[29], [31], [34],

$$\mathbf{F}\left(\mathbf{V}_\beta\right) \sim \left\|\langle \mathbf{v}_\beta \rangle\right\|^2. \quad (19)$$

The correction to Darcy's law in the steady inertial regime is often relatively small (but it can be measured with accurate experimental data [35]–[37]). In many situations, only the quadratic correction has a significant impact and inertial effects are often well *approximated* macroscopically by a quadratic term, i.e.,

$$\mathbf{F}\left(\mathbf{V}_\beta\right) \sim \left\|\langle \mathbf{v}_\beta \rangle\right\|. \quad (20)$$

This is supported by experimental data [33], [35]–[39] as well as numerical predictions [31], [40]. However, from a fundamental perspective, the quadratic expression of the drag is only an approximate description of momentum transport. Calculations over simple unit cells [31] indicate that there are, in fact, many transitional regimes. This implies that, in general, a careful analysis of the regime and the accuracy required in a specific application must be performed before deciding whether to use a simple quadratic correction or more complex descriptions.

The above expression of macro-scale momentum transport, which involves a tensorial expression of $\mathbf{F}$, also suggests the potential existence of anisotropy effects for the Forchheimer term. Simpler expressions are often used in the engineering practice, like Ergun's equation [35] which reads

$$0 = -\nabla P_\beta + \rho_\beta \mathbf{g} - \mu_\beta K^{-1} \mathbf{V}_\beta - \rho_\beta \eta^{-1} \left\|\mathbf{V}_\beta\right\| \mathbf{V}_\beta, \quad (21)$$

where η is called the *passability*. Based on collected experimental data, Ergun proposed the following correlations for K and η in the case of packed beds which are used frequently in the engineering practice

$$K = \frac{\varepsilon^3 d^2}{h_K \left(1-\varepsilon\right)^2} \quad ; \quad \eta = \frac{\varepsilon^3 d}{h_\eta \left(1-\varepsilon\right)}, \quad (22)$$

where d is the equivalent particle diameter and $h_K = 150$ and $h_\eta = 1.75$. Such formulas must be corrected for particles that are not spherical, as shown in [37].

In conclusion, Forchheimer's law is an attractive macro-scale model that is broadly used to study many problems [41]–[45], but it also has its limitations, in particular regarding the expression of the quadratic drag law, as discussed above.

Toward turbulence in porous media

When the Reynolds number becomes very large, a fundamental question is whether the flow can structure on large length scales, larger than several pores, or whether the porous structure imposes a cut-off in the cascade of length scales. This is important because this implies very different macro-scale models. If the vortices and turbulent structures are localized in a single unit-cell, then we may be able to use the general Forchheimer equation, only adapting the form of the drag (see [30], [46]). If this is not the case, the macro-scale model will need to account for other effects. For instance, are terms in $\mathbf{V}_\beta \cdot \nabla \mathbf{V}_\beta$ or macroscale turbulence models needed? Direct numerical simulations in [47] indicate that spatial correlations of the velocity field decrease very rapidly and that the flow is almost periodic. This suggests that the porous medium indeed induces a cut-off in the length scales characterizing the structures of the flow. Therefore, performing calculations of the flow over several unit-cells with periodic boundary conditions will reproduce accurately the flow. On the other hand, it has been observed using direct numerical simulations that turbulence generated in a fluid

layer or at the interface between fluid and porous layers may penetrate a distance of several unit cells into the porous domain and that in this area a macro-scale turbulence model is needed [48]. Transition and bifurcations may also be a lot more sensitive upon the size of the domain considered, as is shown for the unsteady transition in [49], and calculations over a single unit-cell do not yield accurate results for the critical Reynolds numbers. There are still very few studies on this problem and these seminal works open the way toward understanding and modeling truly turbulent situations.

At any rate, for large Reynolds numbers, temporal and spatial fluctuations are both important and time averaging must also be introduced. While the operators for spatial and time averaging may in principle commute [50], the application in a sequential manner, as illustrated below

$$\text{I. } \mathbf{v}_\beta \rightarrow \langle \mathbf{v}_\beta \rangle \rightarrow \overline{\langle \mathbf{v}_\beta \rangle} \tag{23}$$

$$\text{II. } \mathbf{v}_\beta \rightarrow \overline{\mathbf{v}_\beta}\ (RANS, \ldots) \rightarrow \langle \overline{\mathbf{v}_\beta} \rangle, \tag{24}$$

where RANS stands for Reynolds-averaged Navier–Stokes equations, $\langle \varphi \rangle$ stands for the spatial averaging of a variable φ while $\overline{\varphi}$ stands for the time average, may lead to different macro-scale models. The fundamental reason is that each upscaling or averaging step introduces approximations that do not in general commute. Scheme I, favored by [51] and [52] among others, involves first spatial averaging and then, assuming that the closed macro-scale equations have the form of a generalized Forchheimer equation, it is subsequently time averaged. Since it was found that the assumption of a Forchheimer equation is difficult to justify theoretically, most researchers follow scheme II. In this case, it is assumed that the Navier–Stokes equations may be time averaged and the resulting equations are then spatially averaged [50], [53]–[55]). The result is in general some sort of effective RANS (Reynolds-averaged Navier–Stokes equations) macro-scale model. It must be emphasized that, in the two procedures, it is difficult to justify the possibility of a decoupled closure for both averages. Also, a complete validation through experiments or numerical modeling is still an open problem and the need for such models requires to be fully assessed.

Meso-scale models for one-phase flow with pore-scale rough surfaces

In many geometries, the simple multi-scale scheme illustrated in Figure 1 cannot be used directly in direct numerical simulations or in the upscaling algorithms because of the existence of sub-scale heterogeneities. This is the case for instance if the solid–fluid interface displays roughnesses of wavelengths much smaller than the pore-scale characteristic length, l_β, as is illustrated in Figure 3.

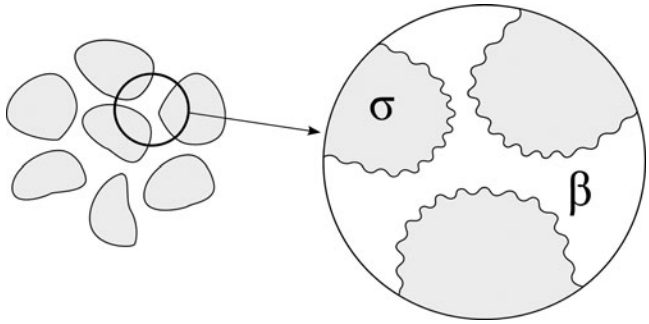

Figure 3. Porous medium with rough surfaces (from [32]).

In that case, one approach consists in developing a meso-scale model, intermediate between the pore-scale and the Darcy-scale. The idea is illustrated in Figure 4. The picture on the left-hand side shows the pore-scale with the flow of the fluid satisfying a no-slip condition on the rough solid–fluid interface. If the impact of the roughness is localized to the vicinity of the wall, and if several other assumptions are satisfied (see [32] for more detail), the complex flow field near the rough interface can be approximated. When that is the case, the flow problem can be replaced by a meso-scale representation involving a smooth effective surface. The boundary condition applying to this surface is an effective boundary condition constructed so that the bulk flow in the pores is correctly approximated by the effective surface modeling. This smooth modeling is illustrated in Figure 4 (right). Various methodologies have been proposed to develop such effective boundary conditions. For the case of Navier–Stokes equations, the reader is referred to works in [56], [57], [58], and [32]. In these studies, the effective boundary condition becomes a generalized, anisotropic Navier conditions which may be written as

$$\mathbf{v}_s = \mathbf{M} \cdot \left[\mathbf{n} \cdot \left(\nabla \mathbf{v}_s + (\nabla \mathbf{v}_s)^T \right) \cdot (\mathbf{I} - \mathbf{nn}) \right], \tag{25}$$

which is satisfied on the smooth effective surface. Here, $\mathbf{v}_s$ is the velocity on the effective surface, $\mathbf{n}$ is the normal to the interface, $\mathbf{I}$ is the unity tensor, and $\mathbf{M}$ is the Navier tensor. The Navier tensor can be obtained from the resolution

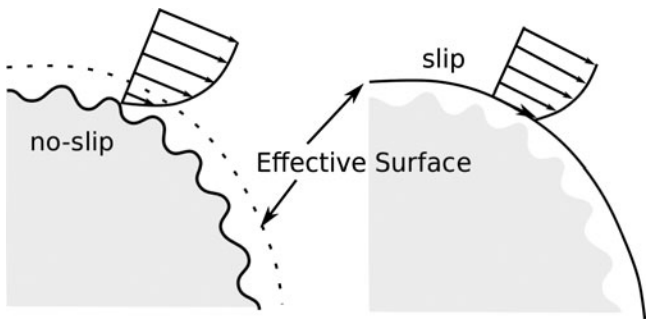

Figure 4. Porous medium with small-scale rough surfaces: rough (left) and effective surface simulation (right), adapted from [32].

of an ancillary problem over a representative portion of the roughness. This tensor depends on the position of the effective surface, which can be fixed arbitrarily—although there is an optimal position minimizing the error [32], [57]. In general, the tensor does not reduce to a scalar, for instance, in the case of anisotropic corrugated surfaces [32]. This theory has been applied to simple unit cells and structured packings with rough surfaces. The results, compared with direct numerical simulations, suggest that the approach is accurate in the weak and strong inertial regime, but fails when unsteady flow develops. When this happens the effect of the roughness is not localized to a boundary layer, but propagates through the whole pore, an effect that cannot be captured by the effective surface. Of course, this is for roughnesses that are larger than the laminar sublayer, otherwise the effect remains localized.

The development of such meso-scale models is a very attractive methodology to deal with highly complex multiple-scale pore structures. This approach will also be discussed in the case of two-phase flows.

Two-phase flow

The pore-scale problem for two-phase flows in porous media involves mass and momentum balance equations for both phases, denoted β and γ, and boundary conditions. For simplicity and clarity, the full upscaling problem is not developed here. However, it is interesting to detail just the condition at the interface between both fluids, in order to present the physics of the problem and links with upscaling. The boundary condition for the momentum equation reads

$$\begin{aligned} &-\mathbf{n}_{\beta\gamma}p_\beta+\mu_\beta\mathbf{n}_{\beta\gamma}\cdot\left(\nabla\mathbf{v}_\beta+\left(\nabla\mathbf{v}_\beta\right)^T\right)= \\ &-\mathbf{n}_{\beta\gamma}p_\gamma+\mu_\gamma\mathbf{n}_{\beta\gamma}\cdot\left(\nabla\mathbf{v}_\gamma+\left(\nabla\mathbf{v}_\gamma\right)^T\right) \\ &+2\sigma H_{\beta\gamma}\mathbf{n}_{\beta\gamma}\text{ at }A_{\beta\gamma}, \end{aligned} \tag{26}$$

where σ is the interfacial tension, $H_{\beta\gamma}$ is the interface curvature, and $\mathbf{n}_{\beta\gamma}$ is the normal. During upscaling using volume averaging, we often need to evaluate the effects of all points $\mathbf{x}+\mathbf{y}$ in the averaging volume on the average value of the field at the centroid $\mathbf{x}$. To do so, we can introduce Taylor series approximation (when the average field is differentiable [18], [19], [23]). For instance, the pressure reads

$$\begin{aligned} &p_\beta\left(\mathbf{x}+\mathbf{y}_\beta\right) \\ &=\left(P_\beta\big|_{\mathbf{x}}+\mathbf{y}_\beta\cdot\nabla P_\beta\big|_{\mathbf{x}}+\mathcal{O}\left(\mathbf{y}_\beta^2\right)\right)+\tilde{p}_\beta\left(\mathbf{x}+\mathbf{y}_\beta\right), \end{aligned} \tag{27}$$

where $\mathbf{y}_\beta$ describes the position of a point in the β-phase relative to the centroid of some averaging volume at position $\mathbf{x}$. Neglecting second-order terms in $\mathcal{O}(\mathbf{y}_\beta^2)$, the boundary condition then reads

$$\begin{aligned} &\mathbf{n}_{\beta\gamma}\left(P_\gamma\big|_{\mathbf{x}}-P_\beta\big|_{\mathbf{x}}\right)+\mathbf{n}_{\beta\gamma}\mathbf{y}_\beta \\ &\quad\cdot\left[\left(\nabla P_\gamma\big|_{\mathbf{x}}-\rho_\gamma\mathbf{g}\right)-\left(\nabla P_\beta\big|_{\mathbf{x}}-\rho_\beta\mathbf{g}\right)+\left(\rho_\gamma-\rho_\beta\right)\mathbf{g}\right] \\ &=-\mathbf{n}_{\beta\gamma}\left(\widetilde{p}_\gamma-\widetilde{p}_\beta\right)+\mu_\gamma\mathbf{n}_{\beta\gamma}\cdot\left(\nabla\mathbf{v}_\gamma+\left(\nabla\mathbf{v}_\gamma\right)^T\right) \\ &\quad-\mu_\beta\mathbf{n}_{\beta\gamma}\cdot\left(\nabla\mathbf{v}_\beta+\left(\nabla\mathbf{v}_\beta\right)^T\right) \\ &\quad+2\sigma H_{\beta\gamma}\mathbf{n}_{\beta\gamma}\text{ on }A_{\beta\gamma}. \end{aligned} \tag{28}$$

Here, we see that the curvature within the averaging volume will depend on (i) the capillary pressure $(P_\gamma|_{\mathbf{x}}-P_\beta|_{\mathbf{x}})$, (ii) gravity effect, (iii) viscous effects, (iv) dynamic effects (important values of the pressure deviations related to the flow or of terms like $(\nabla P_\gamma|_{\mathbf{x}}-\rho_\gamma\mathbf{g})-(\nabla P_\beta|_{\mathbf{x}}-\rho_\beta\mathbf{g})$). Further, another important parameter that does not appear when considering the pointwise fluid–fluid boundary condition is the wettability of the solid phase, which can deeply influence the spatial distribution of the two phases in the pore-space, invasion patterns, and the curvature of the interface [59], [60]. Depending on the assumptions used in the upscaling, several models can be developed. Their physical meaning and mathematical structure are discussed in the next sections.

Quasistatic models for low capillary, Bond and Reynolds numbers

The first class of models that we consider assumes that the boundary condition Eq. (28) can be replaced, for small capillary and Bond numbers (surface tension dominated) defined as

$$\mathrm{Ca}=\frac{\mu_r U_r}{\sigma}\qquad;\qquad\mathrm{Bo}=\frac{\left|\left(\rho_\beta-\rho_\gamma\right)g\right|r_0^2}{\sigma}, \tag{29}$$

by

$$P_\gamma\big|_{\mathbf{x}}-\ P_\beta\big|_{\mathbf{x}}=2\sigma H_{\beta\gamma}. \tag{30}$$

As a result, the interface curvature is considered locally constant. We further assume that the temporal evolution of the interface at the pore-scale is fast compared to that of macro-scale phenomena, i.e., that characteristic times of the interface movement are small compared to the relaxation of the pressure and velocity field at macro-scale. Under such a *quasistatic* assumption, we can introduce a macro-scale capillary pressure condition as

$$P_\gamma-\ P_\beta=p_c(S_\beta,\ldots), \tag{31}$$

where p_c is the capillary pressure relationship, S_β is the saturation defined by Eq. (6) and "..." is here as a reminder that the capillary pressure can depend on other macro-scale parameters. Triple line and wettability effects

are taken into account in the expressions for the capillary and relative permeability, which are treated as nonlinear functions of the saturation. The quasistatic assumption is a hypothesis underlying most heuristic generalized Darcy's laws model classically used in engineering practice [2]. The whole model reads (with also Eq. (31))

$$\frac{\partial \varepsilon S_\beta}{\partial t} + \nabla \cdot \mathbf{V}_\beta = 0 \tag{32}$$

$$\mathbf{V}_\beta = -\frac{1}{\mu_\beta}\mathbf{K}_\beta \cdot \left(\nabla P_\beta - \rho_\beta \mathbf{g}\right) \tag{33}$$

$$\frac{\partial \varepsilon S_\gamma}{\partial t} + \nabla \cdot \mathbf{V}_\gamma = 0 \tag{34}$$

$$\mathbf{V}_\gamma = -\frac{1}{\mu_\gamma}\mathbf{K}_\gamma \cdot \left(\nabla P_\gamma - \rho_\gamma \mathbf{g}\right) \tag{35}$$

$$S_\beta + S_\gamma = 1 \tag{36}$$

with phase permeabilities generally written with relative permeabilities $k_{r\beta}(S_\beta)$ and $k_{r\gamma}(S_\gamma)$ as

$$\mathbf{K}_\beta = \mathbf{K}\, k_{r\beta}(S_\beta) \qquad ; \qquad \mathbf{K}_\gamma = \mathbf{K}\, k_{r\gamma}(S_\gamma). \tag{37}$$

The actual repartition of the phases within a porous medium is necessarily a *transient process* and the quasistatic assumption is not always valid. Transitions between steady-states, and therefore the steady-states themselves, are affected by a variety of dynamic mechanisms such as Haines jumps [61], [62], snap-off [63], [64], viscous entrainment of droplets through constrictions [65], and a variety of other mechanisms [66], [67]. As a consequence, relative permeabilities and capillary pressures, even in the quasistatic assumption, show memory and hysteresis properties and the saturation is not the only state variable [68]. For example, using volume averaging and principles of the thermodynamics of irreversible processes, several authors proposed to use the interfacial area, $a_{\beta\gamma}$, defined as

$$a_{\beta\gamma} = \frac{1}{V}\int_{A_{\beta\gamma}} dA \tag{38}$$

as an additional independent variable [69]–[72].

From an upscaling point of view, the major consequence of these various mechanisms is that the pore-scale repartition of the phases involves several time and length scales, with different flow patterns affecting more than a single pore. This is most obvious when studying meso-scale representations of a porous medium, in particular network models [73]—even though there is also an issue of representativity of a network model as being a realistic representation of complex porous media such as rocks. Recall that, in the absence of macro-scale inertia terms (i.e., very small Reynolds numbers, while one should not forget that many pore-scale mechanisms, such as Haines jumps, may exhibit inertial effects in the transition from one quasistatic state to another) and gravity effects (small Bond numbers), the flow pattern depends on a capillary number and the viscosity ratio, as well as other geometrical and topological characteristics of the network model, including its large-scale length. Results show different flow patterns including viscous fingering, stable displacement, capillary fingering as illustrated by the Ca-viscosity ratio diagrams published in [59], [74] and other works including [60]. The consequence of this complexity is that it is difficult to develop a formal upscaling methodology for all cases.

For example, if we keep the viscosity terms in Eq. (28) while making the assumption of quasistaticity, small Bond and Reynolds numbers, [26], [75]–[78] macro-scale momentum balance equations read

$$\mathbf{V}_\alpha = -\frac{1}{\mu_\alpha}\mathbf{K}_{\alpha\alpha} \cdot \left(\nabla P_\alpha - \rho_\alpha \mathbf{g}\right) + \mathbf{K}_{\alpha\kappa} \cdot \mathbf{V}_\kappa \qquad \alpha, \kappa = \beta, \gamma \qquad \alpha \neq \kappa, \tag{39}$$

which are different from the classical Generalized Darcy's laws. In particular, the cross terms $\mathbf{K}_{\alpha\kappa}$ in these equations account for the viscous interaction between the fluid phases. These cross terms further satisfy the following relations:

$$\mu_\beta \mathbf{K}_{\beta\gamma} \cdot \mathbf{K}_{\gamma\gamma} = \mu_\gamma \mathbf{K}_{\beta\beta} \cdot \mathbf{K}_{\gamma\beta}^T. \tag{40}$$

These equations can also be rearranged into the following form [78]

$$\mathbf{V}_\beta = -\frac{1}{\mu_\beta}\mathbf{K}^*_{\beta\beta} \cdot \left(\nabla P_\beta - \rho_\beta \mathbf{g}\right) - \frac{1}{\mu_\gamma}\mathbf{K}^*_{\beta\gamma} \cdot \left(\nabla P_\gamma - \rho_\gamma \mathbf{g}\right) \tag{41}$$

$$\mathbf{V}_\gamma = -\frac{1}{\mu_\gamma}\mathbf{K}^*_{\gamma\gamma} \cdot \left(\nabla P_\gamma - \rho_\gamma \mathbf{g}\right) - \frac{1}{\mu_\beta}\mathbf{K}^*_{\gamma\beta} \cdot \left(\nabla P_\beta - \rho_\beta \mathbf{g}\right), \tag{42}$$

where the new multiphase permeability tensors are given by

$$\mathbf{K}^*_{\beta\beta} = \left[\mathbf{I} - \mathbf{K}_{\beta\gamma} \cdot \mathbf{K}_{\gamma\beta}\right]^{-1} \cdot \mathbf{K}_{\beta\beta} \tag{43}$$

$$\mathbf{K}^*_{\beta\gamma} = \left[\mathbf{I} - \mathbf{K}_{\beta\gamma} \cdot \mathbf{K}_{\gamma\beta}\right]^{-1} \cdot \left(\mathbf{K}_{\beta\gamma} \cdot \mathbf{K}_{\gamma\gamma}\right) \tag{44}$$

$$\mathbf{K}^*_{\gamma\beta} = \left[\mathbf{I} - \mathbf{K}_{\gamma\beta} \cdot \mathbf{K}_{\beta\gamma}\right]^{-1} \cdot \left(\mathbf{K}_{\gamma\beta} \cdot \mathbf{K}_{\beta\beta}\right) \tag{45}$$

$$\mathbf{K}^*_{\gamma\gamma} = \left[\mathbf{I} - \mathbf{K}_{\gamma\beta} \cdot \mathbf{K}_{\beta\gamma}\right]^{-1} \cdot \mathbf{K}_{\gamma\gamma}. \tag{46}$$

The reciprocity relation Eq. (40) becomes

$$\mu_\beta \mathbf{K}^*_{\beta\gamma} = \mu_\gamma \mathbf{K}^{*T}_{\gamma\beta}. \tag{47}$$

These equations are obtained following the upscaling framework described in Section One-phase flow. Representations of the deviations have a structure similar (albeit extended to two phases) to Eq. (16), and closure problems are similar to the one described in the Appendix.

The permeability tensors in Eqs. (39) or (42) can also be calculated from closure variables (see [26] and [78] for a detailed description).

The importance attributed to cross terms has been the subject of multiple controversies [76], [77], [79]–[81]. So far, these coupling terms have been discarded in applications related to petroleum engineering and many other fields. In low permeability rocks with a large variance of the pore sizes, this may be the consequence of the wetting phase having a tendency to flow in pores of small diameter while the non-wetting phase will flow in large pores. This phase repartition tends to minimize the interfacial area between the fluid phases, thus decreasing the importance of cross terms relative to the friction occurring at the solid/liquid interface. This may explain why measurements in media with a relatively low permeability have produced low values of the cross terms [80].

But the cross terms cannot be discarded in more structured media with high permeability. For instance, they can be computed for flow in capillaries of square [69], [77] or circular [82] sections. Assuming annular flow of two phases in a tube of radius R, as is illustrated in Figure 5, we can derive analytically the effective permeabilities. In the limit $\frac{\mu_\gamma}{\mu_\beta} \ll 1$ [83], we get

$$K_{\beta\beta} \approx K(1 - S_\gamma)^3 \tag{48}$$

$$K_{\beta\gamma} \approx \frac{\mu_g}{\mu_l} \frac{(1 - S_\gamma)^2}{S_\gamma} \tag{49}$$

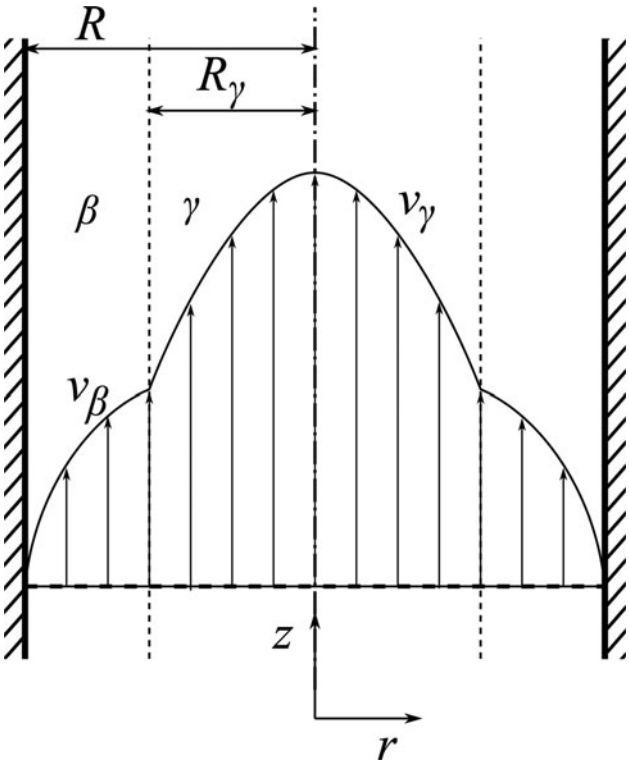

Figure 5. Schematic representation of an annular creeping two-phase flow.

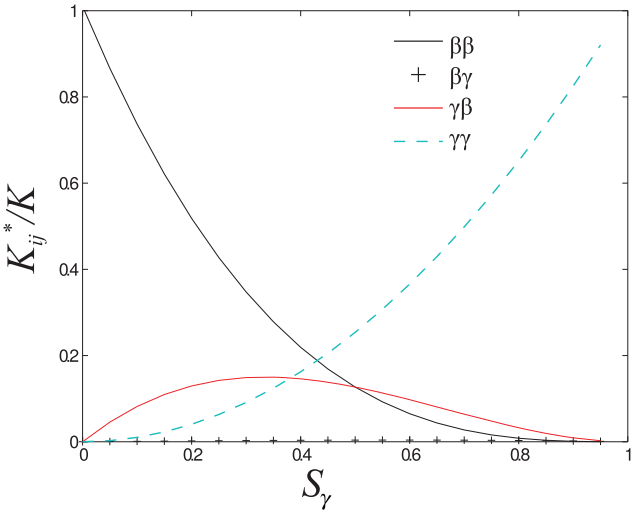

Figure 6. Plot of the different ratios K_{ij}/K for $\frac{\mu_\gamma}{\mu_\beta} = 0.001$.

$$K_{\gamma\gamma} \approx KS_\gamma^2 \tag{50}$$

$$K_{\gamma\beta} \approx \frac{S_\gamma}{1 - S_\gamma}, \tag{51}$$

where $K = \frac{R^2}{8}$ is the tube permeability. Using the transformations provided by Eqs. (43) through (46), we have plotted the effective parameters in Figure 6. Importantly, we see that the permeability cross terms, $K_{\gamma\beta}^*$, are not negligible compared to the standard permeabilities. It was also emphasized recently that they account for a drag force necessary to explain the retention of water observed in a vertical column subject to an upward gas flow in the case of a high permeability medium [34], [83]–[87]. This effect is particularly important in chemical engineering or in nuclear safety (debris bed reflooding) applications. This question will be further discussed in Section Macro-scale models with inertial effects.

Macro-scale dynamic models

To get rid of the constraining assumptions of the previous section, in particular the quasistatic assumption, several studies have proposed dynamic models which can be summarized as follows:

1. Dynamic effects can be captured by introducing additional nonlinear dependencies in the capillary pressure and relative permeabilities, which are called pseudo-functions [88]–[92]. This approach is mostly used in petroleum engineering,
2. Several models account for dynamic effects induced by Darcy-scale heterogeneities and multi-zones [93], multi-zones [94], meniscus propagation [95],

3. The theory of irreversible thermodynamics yields models where the specific area of the fluid–fluid interface becomes a primary variable [69–72],
4. Macro-scale versions of Cahn–Hilliard models have also been proposed [96].

This is beyond the scope of this review to provide a comprehensive literature survey of dynamic models. Here, our goal is essentially to emphasize that, besides differences in the mathematical structure, dynamic effects are often captured by introducing additional dependencies of the effective properties upon terms related to the flow velocity, gravity, and transient effects. As an example, the equations from [93] read

$$\begin{aligned}\mathbf{V}_\beta = &-\frac{1}{\mu_\beta}\mathbf{K}_\beta^* \cdot \left(\nabla P_\beta - \rho_\beta \mathbf{g}\right) - \mathbf{u}_\beta^* \frac{\partial \varepsilon S_\beta}{\partial t} \\ &-\mathbf{U}_\beta^* \cdot \nabla \frac{\partial \varepsilon S_\beta}{\partial t} - \frac{1}{\mu_\beta}\mathbf{M}_\beta^* : \nabla\nabla P_\beta \\ &-\frac{1}{\mu_\beta}\mathbf{\Phi}_\beta - \frac{1}{\mu_\beta}\mathbf{R}_\beta^* : \nabla \mathbf{\Phi}_\beta \end{aligned} \tag{52}$$

for the β-phase macro-scale momentum equation and

$$p_c = \mathcal{F}\left(S_\beta, \left(\rho_\gamma - \rho_\beta\right)\mathbf{g}, \nabla P_\beta, \frac{\partial \varepsilon S_\beta}{\partial t}, \ldots\right) \tag{53}$$

for the capillary pressure relationship. Here, several terms have been introduced to account for dynamic effects. $\mathbf{\Phi}_\beta$ is a source of momentum due to the heterogeneities (see Eq. (2.28) in [93]), new effective properties ($\mathbf{u}_\beta^*$, $\mathbf{U}_\beta^*$, $\mathbf{M}_\beta^*$, $\mathbf{R}_\beta^*$) have been introduced and a gravity term is present to account for large Bond numbers. Similar theoretical results from [69], [71] are available with, besides an equation for the evolution of the interfacial specific area, a capillary pressure relationship with a relaxation term such as

$$P_\gamma - P_\beta = p_c - L_1 \frac{\partial \varepsilon S_\beta}{\partial t}, \tag{54}$$

where L_1 is a phenomenological parameter.

Before going on to discuss inertia effects in the macro-scale models, we want to make a fundamental remark. Most models in the literature are based on quasistatic assumptions, which are not always satisfied by the micro-scale physics. Even if time appears explicitly in several dynamic models, the underlying assumption is that the motion of the interface is relatively slow, so that only spatial averaging is needed to derive macro-scale equations. Why then are these quasistatic models so popular and why are they satisfactory in many cases? We believe that there is more to this problem. One hypothesis is that, since meso-scale results have shown that a macro-scale representative state requires a large number of pores, some ergodicity between time and space averaging is at play. Hence, just averaging in space may be sufficient to smooth out high-frequency fluctuations of the pore-scale fields in time and space. If this hypothesis of ergodicity is incorrect, then this probably means that averaging must be performed in space and time: a great scientific challenge for future research.

Macro-scale models with inertial effects

So far, the most complicated dynamic models (see Section Macro-scale dynamic models) have not been extended for flows with strong inertia effects. The simplest proposals to take these effects into account are based on variants [97], [98] of a generalized Ergun's law, such as

$$0 = -\nabla P_\beta + \rho_\beta \mathbf{g} - \mu_\beta \frac{1}{K\, k_{r\beta}}\mathbf{V}_\beta - \frac{\rho_\beta}{\eta\, \eta_\beta}\left\|\mathbf{V}_\beta\right\| \mathbf{V}_\beta, \tag{55}$$

where $k_{r\beta}$ is the relative permeability of the β-phase and where the Forchheimer term involves a relative passability η_β. A similar equation may be written for the γ-phase. The effective parameters, $k_{r\beta}$ and η_β, depend on the saturation and are often assigned the following forms:

$$k_{r\beta} = \left(1 - S_\gamma\right)^n \quad ; \quad \eta_\beta = \left(1 - S_\gamma\right)^m \tag{56}$$

$$k_{r\gamma} = S_\gamma^p \quad ; \quad \eta_\gamma = S_\gamma^q \tag{57}$$

with different values for the exponents [99]–[101].

While this form may account for the increase in pressure drop due to inertial effects, it does not fully describe the drag between both phases and the resulting retention effects. Several models have been proposed to reproduce fluid–fluid interactions, for instance, [86] proposed the following equations (the original equations have been casted into a form suitable for comparison with generalized Darcy's law):

$$\begin{aligned} 0 = &-\nabla P_\beta + \rho_\beta \mathbf{g} - \mu_\beta \frac{1}{K\, k_{r\beta}}\mathbf{V}_\beta \\ &-\frac{\rho_\beta}{\eta\, \eta_\beta}\left\|\mathbf{V}_\beta\right\| \mathbf{V}_\beta + \frac{\mathbf{F}_{\beta\gamma}^S}{\varepsilon S_\beta} \end{aligned} \tag{58}$$

$$\begin{aligned} 0 = &-\nabla P_\gamma + \rho_\gamma \mathbf{g} - \mu_\beta \frac{1}{K\, k_{r\beta}}\mathbf{V}_\beta \\ &-\frac{\rho_\beta}{\eta\, \eta_\beta}\left\|\mathbf{V}_\beta\right\| \mathbf{V}_\beta - \frac{\mathbf{F}_{\beta\gamma}^S}{\varepsilon(1 - S_\beta)}, \end{aligned} \tag{59}$$

where the term $\mathbf{F}_{\beta\gamma}^S$ accounts for the interfacial interaction.

A generalized form of two-phase flow equations accounting for cross terms and inertia effects has been obtained theoretically through upscaling by [102] and reads

$$\begin{aligned} \mathbf{V}_\alpha = &-\frac{1}{\mu_\alpha}\mathbf{K}_\alpha \cdot \left(\nabla P_\alpha - \rho_\alpha \mathbf{g}\right) - \mathbf{F}_{\alpha\alpha} \cdot \mathbf{V}_\alpha \\ &+ \mathbf{K}_{\alpha\kappa} \cdot \mathbf{V}_\kappa - \mathbf{F}_{\alpha\kappa} \cdot \mathbf{V}_\kappa \qquad \alpha, \kappa = \beta, \gamma \quad \alpha \neq \kappa. \end{aligned} \tag{60}$$

The first two terms in the right-hand side of these equations correspond to a fully anisotropic generalization of the multiphase Ergun's law. The third term corresponds to viscous interactions, as already discussed in Section Quasistatic models for low capillary, Bond, and Reynolds numbers, and the last term is a cross term mainly associated with the inertial correction. These models require the determination of several effective properties which depend nonlinearly upon saturations and velocities, as well as on the viscosity ratio and geometrical features of the porous space. All these dependencies are not well understood today and determining these effective properties from direct numerical simulations or experiments remains an open problem and a challenging task.

To illustrate the capabilities of the various models, let us consider two-phase flow in a vertical column of high permeability (and hence small capillary effects). Initially, the porous medium is saturated by a liquid phase, β, and an upward flow of a gas phase, γ, is imposed. The fluid phase will be progressively ejected by the top of the column until the situation reaches steady-state and $\mathbf{V}_\beta = 0$. Using the more general form Eq. (60), we have that

$$0 = -\frac{1}{\mu_\beta} K_\beta \left(\frac{\partial P_\beta}{\partial z} - \rho_\beta \mathbf{g} \cdot \mathbf{e}_z \right) + \left(K_{\beta\gamma} - F_{\beta\gamma} \right) V_\gamma . \tag{61}$$

On the other hand, using only the classical generalized Darcy's laws, i.e., $(K_{\beta\gamma} - F_{\beta\gamma}) = 0$, one gets

$$\frac{\partial P_\beta}{\partial z} = \rho_\beta \mathbf{g} \cdot \mathbf{e}_z . \tag{62}$$

The result of the generalized Darcy's laws *does not agree* with experimental data [87], [103]. This is illustrated in Figure 7, which represents the data obtained from experiments through a cylindrical porous column by [83], [104], as well as theoretical results. In these experiments, the column was initially saturated by water (β-phase), then gas (γ-phase) was injected from below. Liquid flowed out of

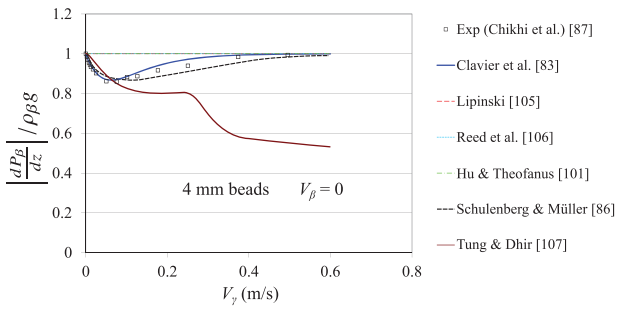

Figure 7. Experimental and modeling results for the normalized pressure drop versus the gas velocity at $V_\beta = 0$ (from Clavier et al. in [104]).

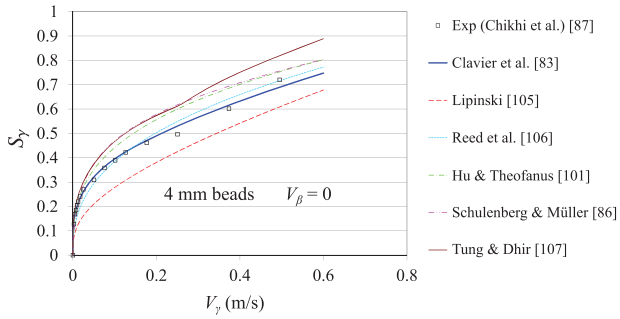

Figure 8. Experimental and modeling results for the gas saturation versus the gas velocity at $V_\beta = 0$ (from Clavier et al. in [104]).

the column from the top until a quasi-steady macro-scale situation was obtained. The figure shows the pressure gradient normalized by the liquid hydrostatic pressure gradient versus the gas velocity, for a liquid average velocity equal to zero. The simple generalized Darcy's law models with Ergun's type inertia term (Eq. (62)), as proposed by [105], [106], or [101], yield completely erroneous results. Below a critical velocity, the fluid is lifted by the gas and has a decreasing apparent weight. This corresponds to the viscous interactions, which in the model are captured by the term involving $K_{\beta\gamma}$. When the velocity is further increased, inertial effects, as taken into account in Eq. (61) by the extra term involving $F_{\beta\gamma}$, tend to reduce the lift and increase the apparent weight.

In summary, keeping the extra terms in Eq. (61) allows to account for liquid retention due to the drag force imposed on the liquid by the upward flow for a large range of Reynolds number. Various expressions have been proposed in the literature for the effective parameters [83], [86], [107] and their application to [87] experiments are reported in Figures 7 and 8. High nonlinearity, lack of data, and the large number of parameters that needs to be determined lead to strong difficulties in the identification procedure. This may explain the discrepancy observed between data and predictions [87], [108], [109] as is shown in Figures 7 and 8 adapted from [87]. Further research is therefore necessary to better parameterize the models.

Two-phase flows: Special models

In this section, we review two-phase flow models that have been proposed to reproduce specific mechanisms observed at high capillary and Bond numbers. In such cases, the time and length-scale constraints which are necessary to develop macro-scale two-phase flow models are not fulfilled. Therefore, specific treatments and assumptions are needed. Two types of models have been proposed and are the subject of current research. They are briefly presented below.

Figure 9. Photograph of structured packings (Wikimedia Commons, author: Luigi Chiesa).

Models with a splitting of phase

Structured packings have been extensively used in the past decades in absorption and distillation columns or chemical reactors. They are often made of assemblies of corrugated metal sheets, alternating the orientation from one sheet to another, thus creating a porous medium having the honeycomb structure illustrated in Figure 9. The resulting material has a relatively high surface area and small pressure drops. The characteristic length for the pores is several millimeters (sometimes up to the centimeter), thus pore-scale flow in such devices is sensitive to effects of gravity and inertia.

Further, the alternating directions of the structure may create preferential flowpaths which are followed by only a portion of the fluid. For such geometries, a single macro-scale equation describing the liquid phase flow is often not very accurate, as it fails to account for the bimodal distribution of flow angles. Models with a liquid phase decomposed into two pseudo-phases, i.e., one macro-scale equation for the gas phase but two macro-scale equations for the liquid, have been proposed to handle such cases [110]–[113]. The result is a set of balance equations for the gas phase (a single effective phase is enough in the context of structured packings), γ, and two sets of balance equations, one for liquid phase part 1, β_1, and one for liquid phase part 2, β_2. For instance, the three mass balance equations read

$$\varepsilon \frac{\partial S_\gamma}{\partial t} + \nabla \cdot \mathbf{V}_\gamma = 0, \tag{63}$$

$$\varepsilon \frac{\partial S_{\beta_1}}{\partial t} + \nabla \cdot \mathbf{V}_{\beta_1} = \dot{m}, \tag{64}$$

$$\varepsilon \frac{\partial S_{\beta_2}}{\partial t} + \nabla \cdot \mathbf{V}_{\beta_2} = -\dot{m}, \tag{65}$$

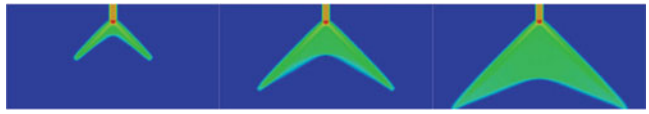

Figure 10. Saturation $S_{\beta_1} + S_{\beta_2}$ showing the spreading at three different times of a top of column impinging jet (from [115]).

where $\dot{m}$ is the mass exchange term which must be modeled in terms of the three "phases" saturations, pressures, and velocities.

While there were attempts to develop these models through volume averaging, part of the resulting models are still heuristic. In particular, the description of the exchange of mass (and momentum) between the two macro-scale liquid phases remains an open problem. To illustrate this, let us consider the spreading of a *single* jet impinging such a porous medium as described by these models (Figures 10 and 11 taken from [113]). We see in Figure 10 that the impinging jet tends to be distributed in two jets along the two directions of the corrugated sheets. On the other hand, exchange between the phases, as expressed by the term $\dot{m}$ in Eqs. (64) and (65), tends to smear out this double jet structure. Depending on the intensity of the exchange term, the two liquid phases show a distinct shape with two separate jets when there is barely no exchange, or a more classical solution when the exchange is strong. These two shapes have been observed experimentally [111], [114]. The results obtained by [114] are presented in Figure 11a. This figure is a plot of $S_{\beta_1} + S_{\beta_2}$ at a given cross-section of the experimental column. It clearly shows the anisotropic spreading of the jet due to the peculiar geometry of the structured medium. Figures 11b to 11h show predictions obtained in [115], for increasing values of the exchange term. These results demonstrate that such models have the potential for representing experimental data. However, the accurate determination of the effective properties needed in such models requires further investigations.

Dynamic meso-scale and hybrid models

In porous media with low capillarity effects, the liquid moves by a series of different mechanisms:

- films developing over the grain surfaces,
- bridges forming between films when close to contact points,
- bulging films due to either instabilities or the effect of high Bond numbers.

This flow complexity is illustrated by the CFD results from [116], which are presented in Figure 12. The results show the spreading of a liquid film from a jet impacting the north pole of the top sphere in a vertical stack. The

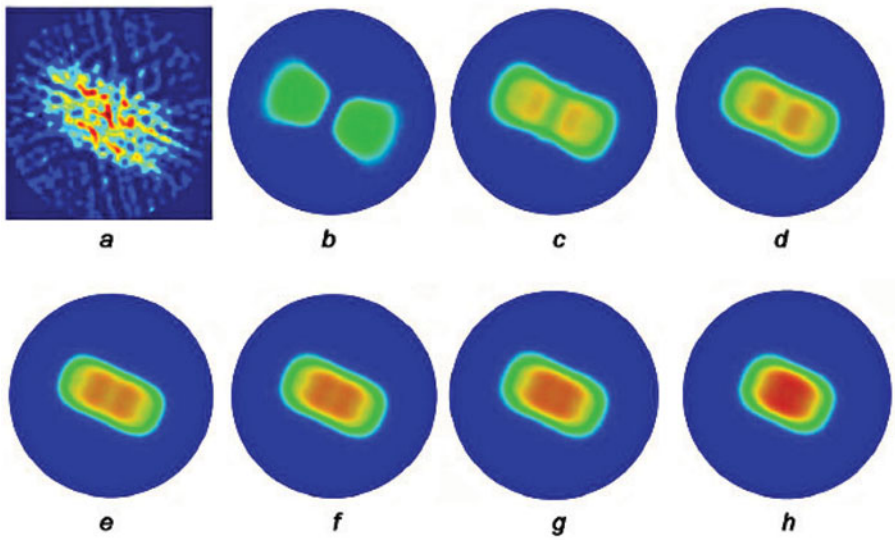

Figure 11. Saturation $S_{\beta_1} + S_{\beta_2}$ showing the spreading at a given column cross-section of an impinging jet at the top of the column (from [113]): a), experimental results from [114], b–h), numerical results with increasing mass exchange from [113].

liquid then spreads as a film, reaches the contact point where films develop on the adjacent spheres, and goes on to the next sphere. As a consequence of the diversity of mechanisms at play, several flow regimes may develop as illustrated, for instance, in [117], [118], [119], and [120]. Such regimes can be easily observed when studying the quasi-2D flow of a liquid in a bundle of cylinders as illustrated in Figure 13 (left) taken from [121]. The porous medium is a micromodel with pillars, and the photograph shows the distribution of phases resulting from a jet impacting the upper part of the cylinder in the middle. The jet spreads laterally because of bulging film contacting adjacent pillars, a mechanism that cannot be described easily at the macro-scale by capillary diffusion effect embedded in the classical Generalized Darcy's laws. In addition, the length-scale constraints (Eq. (1)) necessary to develop a macro-scale theory are not satisfied.

The flow complexity can be captured by direct numerical modeling [122] as illustrated in Figure 13 (right) where the flow between the cylinders is obtained using a Volume of Fluids method [121]. Two limitations arise for a direct application of CFD to complex systems. First, it is difficult to obtain deterministic predictions since many of the mechanisms involved are subject to unpredictability (e.g., instabilities, sensitivity to small geometrical features). Second, it is very difficult to get accurate, converged, and stable numerical solutions, even for a limited number of pores. Nowadays, accurate calculations for a large amount of pores, especially in 3D, is beyond the capabilities of modern computers. Indeed, even for a porous medium with a correlation length of the order of the grain size, the phase repartition pattern develops over dozens of pores. In such cases, we are faced with the following difficulties:

1. The complexity of pore-scale mechanisms and the broad range of time and spatial characteristic scales, make the development of a macro-scale model very difficult to achieve,

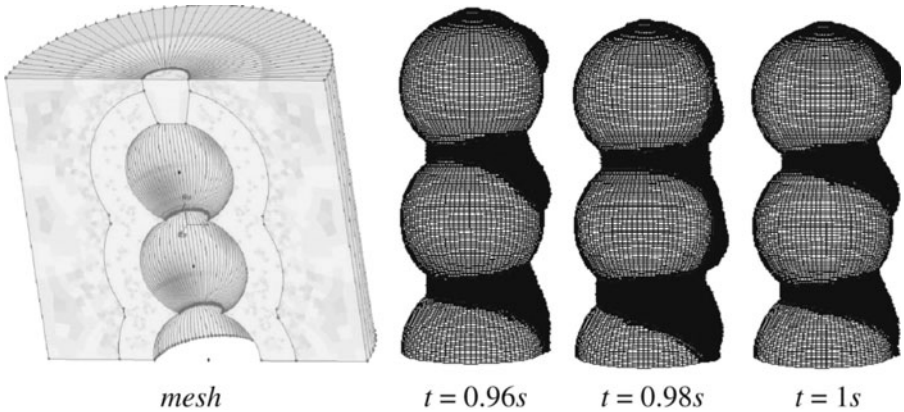

Figure 12. Illustration of 3D simulations for ethanol/alumina systems (mesh and liquid volume fraction snapshots). The fluid flows from the north pole of the top sphere. Taken from [116], Figure 2.

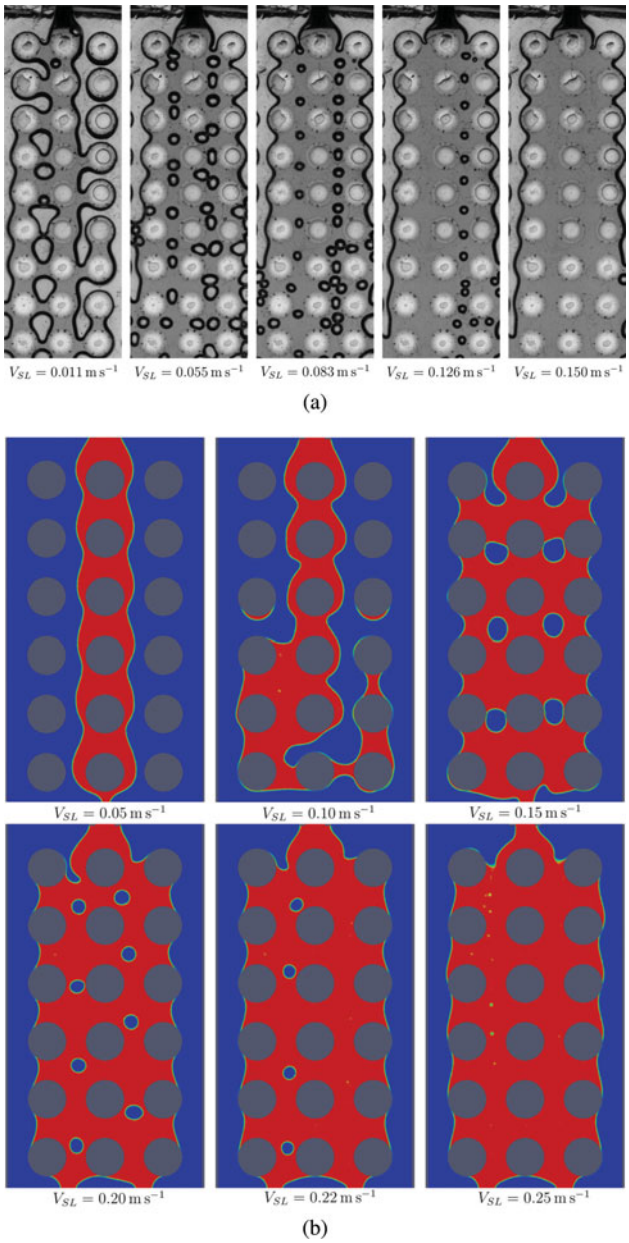

Figure 13. Experimental data (a) and numerical solution (b) for two-phase flow in a bundle of cylinders, from [121].

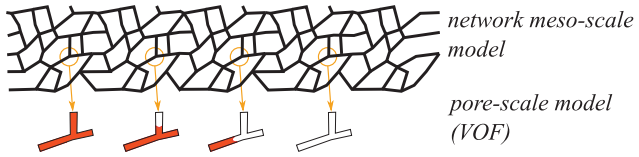

Figure 14. Schematic representation of a mesoscale hybrid model.

2. Direct Numerical Solution (DNS) is equally very difficult to carry on because of the number of pores involved.

As discussed in Section Quasistatic models for low capillary, Bond, and Reynolds numbers, it is often convenient to use a simplified meso-scale description of the porous medium as a pore network model. This is particularly true when complex percolation mechanisms are encountered. Rules describing the flow between and within nodes must be introduced. This is relatively straightforward for classical percolation problems (Poiseuille like pressure drop for describing the flow between nodes and quasistatic capillary effects [73], [123]), but these rules must be adapted for dynamic cases. Dynamic rules may be introduced directly in the network model [40], [120], [124]–[126] under the form of dynamic pressure drop relationships or even a stochastic distribution of the phase entering a node into the adjacent links. These rules can be obtained heuristically, experimentally, or with the help of localized (i.e., over a small number of pores) direct numerical simulations. In that last case, meso-scale simulations are coupled with pore-scale simulations, so that we often refer to such models as *hybrid models*. The idea of such approaches is to couple the pore-network description with local pore-scale simulations carried out with, for instance, a Volume Of Fluid numerical model. The local VOF simulations provides the dynamic rules necessary to advance the fluid flow in the pore network model. This hybrid modeling is schematically illustrated in Figure 14.

As an illustration of the meso-scale approach, Figure 15 represents the saturation and pressure field obtained by [126] for gas–liquid trickle flows inside fixed beds of spherical particles. The geometry is first

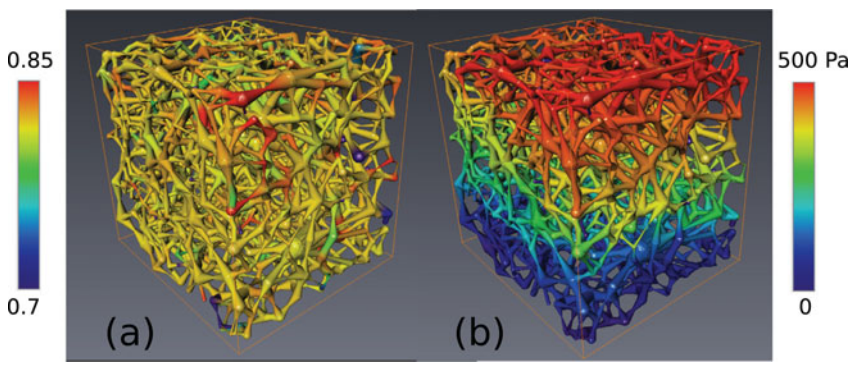

Figure 15. Results from [126] for saturation (a) and pressure (b) fields.

obtained using X-ray micro-tomography. Then the flow in the throats between pores is described using the results for the annular two-phase flow in tubes described in Section Quasistatic models for low capillary, Bond, and Reynolds numbers, i.e., the model with cross terms. Finally, the flow distribution between pores and throats is obtained by solving mass and momentum balance equations. While results are promising, further work is needed to make these models operational in engineering practice. It must also be reminded that meso-scale models need more computational resources than macro-scale representations. Therefore, efforts to obtain more dynamic purely macro-scale models must also continue.

Conclusions

In this paper, we have reviewed one- and two-phase flows in highly permeable porous media, with an emphasis on macro-scale modeling at high Reynolds, capillary, and Bond numbers.

For one-phase flow, we have shown that moderate inertial effects can be captured by modifications of Darcy's law. For large Reynolds numbers, however, when time fluctuations becomes important, there are still many unanswered questions regarding the time averaging procedure, the form of the drag, the localization of the flow structures, and the development of fully macro-scale turbulent models. For two-phase flows in the creeping limit, we have shown that the generalized Darcy's law can be extended to account for couplings between the two phases via cross terms. In the case of high Reynolds numbers, several models were proposed that can be classified in two categories. First, there are extensions of Ergun's one-phase model to the two-phase flow case, with relative permeabilities and passabilities as the main effective parameters. Second, several models with additional interaction terms have been obtained heuristically or via upscaling procedures. These models reproduce the experimental results available with relatively good accuracy. However, it is clear from the comparison between predictions and experimental data that additional work should be done to yield better estimates of the various nonlinear expressions for the effective parameters used in these models. This review also shows that many problems remain largely open for two-phase flow at large Bond and capillary numbers. For this case, classical quasistatic formulations seem to work in the situation where, in theory, they should not, as dynamic effects are important. An hypothesis is that of a time/space ergodicity, which would eliminate the need for temporal averaging, although this needs to be explored more thoroughly. We have also shown that hybrid models have been proposed in the literature, which couple solutions of the problem at different scales. Such formulations represent an interesting alternative to macro-scale models with the potential to be more accurate and capture more dynamic phenomena. Because of their computational cost, they are often limited and cannot supplant macro-scale formulations, but can this change with the advent of high performance computing?

There are also many open problems that are specific to given porous structures, such as those inducing bi-structured flows with almost independent behaviors of different portions of the liquid phase. Models with a splitting of the liquid (or gas) flow into two macro-scale fluids have shown their ability to reproduce results qualitatively but, once again, much work should be devoted to the validation of the mathematical structure of such models and the estimation of the relevant effective transport properties.

Nomenclature

$a_{\beta\gamma}$	specific interfacial area, m^{-1}
$A_{\beta\sigma}$	interface between the fluid and solid phases
$\mathbf{B}$	mapping variable
$\mathbf{b}$	mapping variable, m^{-1}
Bo	Bond number
Ca	capillary number
CFD	Computational fluid dynamics
d	particle diameter, m
DNS	Direct numerical solution
$\mathbf{F}^S_{\alpha\kappa}$	inertia multiphase effective properties
$\mathbf{F}^S_{\beta\gamma}$	interfacial interaction, $\mathrm{Pa}\cdot\mathrm{m}^{-1}$
F	inertia term, $\mathrm{Pa}\cdot\mathrm{s}\cdot\mathrm{m}^{-2}$
g	gravity acceleration, $\mathrm{m}\cdot\mathrm{s}^{-2}$
h_η	passability correction factor
h_k	permeability correction factor
$H_{\beta\gamma}$	interface curvature, m^{-1}
$\mathbf{K}$	intrinsic permeability tensor, m^2
$\mathbf{K}_{\alpha\kappa}$	cross term
$\mathbf{K}^*_{\alpha\kappa}$	modified multiphase permeability tensor, m^2
$k_{r\alpha}$	α-phase relative permeability
L	large-scale characteristic length, m
L_1	phenomenological parameter, $\mathrm{Pa}\cdot\mathrm{s}$
l_σ	pore-scale characteristic length, m
l_p	pore-scale characteristic length, m
$\dot{m}$	mass exchange term, $\mathrm{kg}\cdot\mathrm{m}^{-3}\cdot\mathrm{s}^{-1}$
$\mathbf{M}$	Navier tensor, m
$\mathbf{M}^*_\beta$	new effective property, Eq. (52), $\mathrm{m}^3\cdot\mathrm{s}^{-2}$
V	averaging volume
$\mathbf{n}_{\beta\sigma}$	normal to $A_{\beta\sigma}$
$\tilde{p}_\beta$	pressure deviation, Pa
p_c	capillary pressure, Pa
P_β	intrinsic phase average pressure, Pa
p_β	β-phase pressure, $\mathrm{N}\cdot\mathrm{m}^{-2}$
$\mathbf{R}^*_\beta$	new effective property, Eq. (52), m
r_0	averaging volume characteristic length, m
RANS	Reynolds-averaged Navier–Stokes equations
Re	Reynolds number
S_β	β-phase saturation
t	time, s
$\mathbf{U}_\beta$	β-phase intrinsic velocity, $\mathrm{m}\cdot\mathrm{s}^{-1}$

$\mathbf{U}^*_\beta$	new effective property, Eq. (52)
$\mathbf{u}^*_\beta$	new effective property, Eq. (52), m
U_r	reference velocity, $\mathrm{m}\cdot\mathrm{s}^{-1}$
$\mathbf{V}_\beta$	β-phase filtration velocity, $\mathrm{m}\cdot\mathrm{s}^{-1}$
$\mathbf{v}_\beta$	β-phase velocity, $\mathrm{m}\cdot\mathrm{s}^{-1}$
$\mathbf{v}_s$	velocity on effective surface, $\mathrm{m}\cdot\mathrm{s}^{-1}$
$\mathcal{V}_\beta$	β-phase volume
$\tilde{\mathbf{v}}_\beta$	velocity deviation, $\mathrm{m}\cdot\mathrm{s}^{-1}$
$\mathbf{x}$	current point, m
$\mathbf{y}$	position relative to the centroid of the averaging volume, m

Greek Symbols

β_i	refers to the split β-phase
η	passability, m
η_β	relative passability
γ_β	β-phase indicator
$\langle\psi_\beta\rangle$	β-phase average
$\langle\psi_\beta\rangle^\beta$	β-phase intrinsic average
μ_β	β-phase dynamic viscosity, $\mathrm{Pa}\cdot\mathrm{s}$
$\overline{\psi_\beta}$	time average
ψ_β	β-phase variable
ρ_β	β-phase density, $\mathrm{kg}\cdot\mathrm{m}^{-3}$
σ	interfacial tension, $\mathrm{N}\cdot\mathrm{m}^{-1}$
ε	porosity
ε_β	β-phase volume fraction

Subscripts

β	β-phase property
$\beta\gamma$	refers to $\beta\gamma$ interface
γ	γ-phase property
σ	σ-phase property
p	pore-scale property

Notes on contributors

Yohan Davit is Chargé de Recherche CNRS at the Institut de Mécanique des Fluides in Toulouse, France. Prior to joining CNRS, he was a postdoctoral researcher at the Mathematical Institute at the University of Oxford. He received his Ph.D. degree, for which he was awarded the prize Léopold Escande, in 2011 from the University of Toulouse. He studied at the Institut National Polytechnique de Grenoble and the Université Joseph Fourier, where he obtained his MS degree. His research interests include the ecology of biofilms, transport phenomena in biological and porous media, and multiscale approaches for heterogenous systems.

Michel Quintard is Directeur de Recherche CNRS at the Institut de Mécanique des Fluides in Toulouse, France. Engineer from Top School "Ecole Nationale Supérieure des Arts et Métiers," he received his Ph.D. in fluid mechanics from the University of Bordeaux (1979). His research interests focus on transport phenomena in porous media with fundamental objectives such as the development of macro-scale models through the use of averaging techniques, applied to different scales and different displacement mechanisms (multiphase, multicomponent, phase change, chemical reaction, biodegradation, dissolution, superfluid, …), with applications in petroleum engineering, environmental hydrogeology, chemical engineering, nuclear safety, aerospace industry, etc. M. Quintard has co-authored about 190 papers in archival journals. He was awarded a Bronze Medal from CNRS in 1984, the Prize Coron-Thévenet from Académie des Sciences de Paris in 1994, and became Chevalier of the Légion d'Honneur in 2009 for his action as President of the Scientific Council of IRSN (French Nuclear Safety and Radioprotection Institute).

References

[1] H. Darcy, *Fontaines Publiques de la Ville de Dijon*. Paris, France: Dalmont, 1856.

[2] M. Muskat, *The Flow of Homogeneous Fluids Through Porous Media*, International Series in Physics. New York, USA: The Maple Press Company, 1946.

[3] A. Bourgeat, M. Quintard, and S. Whitaker, "Eléments de Comparaison entre la Méthode d'Homogénéisation et la Méthode de Prise de Moyenne avec Fermeture," *C. R. Acad. Sci., Paris II*, vol. 306, pp. 463–466, 1988.

[4] B. Wood, F. Cherblanc, M. Quintard, and S. Whitaker, "Volume averaging for determining the effective dispersion tensor: Closure using periodic unit cells and comparison with ensemble averaging," *Water Resour. Res.*, vol. 39, no. 6, pp. 1154–1173, 2003.

[5] Y. Davit et al., "Homogenization via formal multiscale asymptotics and volume averaging: How do the two techniques compare?" *Adv. Water Resour.*, vol. 62, pp. 178–206, 2013.

[6] Y. Davit and M. Quintard, "Theoretical analysis of transport in porous media: Multi-equation and hybrid models for a generic transport problem with non-linear source terms," in *Handbook of Porous Media*, K. Vafai, Ed. New York, USA: Taylor & Francis, pp. 245–320, 2015.

[7] C. M. Marle, "Application de la Méthode de la thermodynamique des processus Irréversibles à l'Écoulement d'un fluide à travers un milieux poreux," *RILEM Bull.*, vol. 29, pp. 1066–1071, 1965.

[8] C. M. Marle, "On macroscopic equations governing multiphase flow with diffusion and chemical reactions in porous media," *Int. J. Eng. Sci.*, vol. 20, no. 5, pp. 643–662, 1982.

[9] S. Whitaker, "Diffusion and dispersion in porous media," *AIChE J.*, vol. 13, pp. 420–427, 1967.

[10] S. Whitaker, *The Method of Volume Averaging*. Dordrecht, The Netherlands: Kluwer Academic Publishers, 1999.
[11] W. G. Gray and S. M. Hassanizadeh, "Macroscale continuum mechanics for multiphase porous-media flow including phases, interfaces, common lines and common points," *Adv. Water Resour.*, vol. 21, pp. 261–281, 1998.
[12] J. Bensoussan, L. Lions, and G. Papanicolaou, *Asymptotic Analysis for Periodic Structures*. Amsterdam: North-Holland, 1978.
[13] L. Tartar, *The General Theory of Homogenization: A Personalized Introduction*, Lecture Notes of the Unione Matematica Italiana. Berlin, Germany: Springer, 2009.
[14] J.-L. Auriault, C. Boutin, and C. Geindreau, *Homogenization of Coupled Phenomena in Heterogeneous Media*, vol. 149. London, UK: John Wiley & Sons, 2010.
[15] G. Matheron, *Les Variables Régionalisées et leur Estimation : une Application de la Théorie des Fonctions Aléatoires aux Sciences de la Nature*. Paris: Masson, 1965.
[16] L. W. Gelhar, and M. A. Collins, "General analysis of longitudinal dispersion in nonuniform flow," *Water Resour. Res.*, vol. 7, no. 6, pp. 1511–1521, 1971.
[17] G. Dagan, *Flow and Transport in Porous Formations*. Berlin: Springer-Verlag, 1989.
[18] M. Quintard and S. Whitaker, "Transport in ordered and disordered porous media 1: The cellular average and the use of weighting functions," *Transp. Porous Media*, vol. 14, pp. 163–177, 1994.
[19] M. Quintard and S. Whitaker, "Transport in ordered and disordered porous media 2: Generalized volume averaging," *Transp. Porous Media*, vol. 14, pp. 179–206, 1994.
[20] M. Quintard and S. Whitaker, "Transport in ordered and disordered porous media 3: Closure and comparison between theory and experiment," *Transp. Porous Media*, vol. 15, pp. 31–49, 1994.
[21] M. Quintard and S. Whitaker, "Transport in ordered and disordered porous media 4: Computer generated porous media," *Transp. Porous Media*, vol. 15, pp. 51–70, 1994.
[22] M. Quintard and S. Whitaker, "Transport in ordered and disordered porous media 5: Geometrical results for two-dimensional systems," *Transp. Porous Media*, vol. 15, pp. 183–196, 1994.
[23] Y. Davit and M. Quintard, "Technical notes on volume averaging in porous media I: How is spatial averaging defined for periodic and quasiperiodic structures," *Transp. Porous Media*, vol. 119, no. 3, pp. 555–584, 2017.
[24] G. Chauveteau and C. Thirriot, "Régimes d'Écoulement en milieu poreux et Limite à la Loi de darcy," *La Houille Blanche*, vol. 2, pp. 141–148, 1967.
[25] E. Sanchez-Palencia, "On the asymptotics of the fluid flow past an array of fixed obstacles," *Int. J. Eng. Sci.*, vol. 20, no. 12, pp. 1291–1301, 1982.
[26] S. Whitaker, "Flow in porous media 1: A theoretical derivation of Darcy's law," *Transp. Porous Media*, vol. 1, pp. 3–25, 1986.
[27] J. Wodié and T. Levy, "Correction non Linéaire à la Loi de Darcy," *C. R. Acad. Sci. Paris II*, vol. 312, pp. 157–161, 1991.
[28] C. Mei and J. Auriault, "The effect of weak inertia on flow through a porous medium," *J. Fluid Mech.*, vol. 222, pp. 647–663, 1991.
[29] M. Firdaouss, J. Guermond, and P. Le Quéré, "Non linear corrections to Darcy's law at low Reynolds numbers," *J. Fluid Mech.*, vol. 343, pp. 331–350, 1997.
[30] E. Skjetne and J. Auriault, "High velocity laminar and turbulent flow in porous media," *Transp. Porous Media*, vol. 36, pp. 131–147, 1999.
[31] D. Lasseux, A. Abbasian, and A. Ahmadi, "On the stationary macroscopic inertial effects for one-phase flow in ordered and disordered porous media," *Phys. Fluids*, vol. 23, pp. 1–19, 2011.
[32] S. Pasquier, M. Quintard, and Y. Davit, "Modeling flow in porous media with rough surfaces: Effective slip boundary conditions and application to structured packings," *Chem. Eng. Sci.*, vol. 165, pp. 131–146, 2017.
[33] P. Forchheimer, "Wasserbewegung durch boden," *Z. Ver. Deutsch Ing.*, vol. 45, pp. 1782–1788, 1901.
[34] K. Yazdchi and S. Luding, "Toward unified drag laws for inertial flows through fibrous media," *Chem. Eng. J.*, vol. 207, pp. 35–48, 2012.
[35] S. Ergun, "Fluid flow through packed columns," *Chem. Eng. Progress*, vol. 48, no. 2, pp. 89–94, 1952.
[36] J. Lage, B. Antohe, and D. Nield, "Two types of nonlinear pressure-drop versus flow-rate relation observed for saturated porous media," *Trans. ASME*, vol. 119, pp. 700–706, 1997.
[37] R. Clavier, N. Chikhi, F. Fichot, and M. Quintard, "Experimental investigation on single-phase pressure losses in nuclear debris beds: Identification of flow regimes and effective diameter," *Nucl. Eng. Des.*, vol. 292, pp. 222–236, 2015.
[38] I. MacDonald, M. El-Sayed, K. Mow, and F. Dullien, "Flow through porous media - The ergun equation revisited," *Ind. Eng. Chem. Fundam.*, vol. 18, pp. 199–208, 1979.
[39] L. Li and W. Ma, "Experimental study on the effective particle diameter of a packed bed with non-spherical particles," *Transp. Porous Media*, vol. 89, pp. 35–48, 2011.
[40] F. Larachi, R. Hannaoui, P. Horgue, F. Augier, Y. Haroun, S. Youssef, E. Rosenberg, M. Prat, and M. Quintard, "X-Ray micro-tomography and pore network modeling of single-phase fixed-bed reactors," *Chem. Eng. J.*, vol. 240, pp. 290–306, 2014.
[41] K. Vafai and C. L. Tien, "Boundary and inertia effects on flow and heat transfer in porous media," *Int. J. Heat Mass Trans.*, vol. 24, pp. 195–203, 1981.
[42] M. S. Phanikumar and R. L. Mahajan, "Non-Darcy natural convection in high porosity metal foams," *Int. J. Heat Mass Trans.*, vol. 45, no. 18, pp. 3781–3793, 2002.
[43] F. Fichot, F. Duval, N. Trégourès, C. Béchaud, and M. Quintard, "The impact of thermal non-equilibrium and large-scale 2D/3D effects on debris bed reflooding and coolability," *Nucl. Eng. Des.*, vol. 236, no. 19, pp. 2144–2163, 2006.
[44] S. B. Beale, "A Simple, Effective viscosity formulation for turbulent flow and heat transfer in compact heat exchangers," *Heat Trans. Eng.*, vol. 33, no. 1, pp. 4–11, 2012.
[45] A. Bousri, R. Nebbali, R. Bennacer, K. Bouhadef, and H. Beji, "Numerical investigation of forced convection nonequilibrium effects on heat and mass transfer in porous media," *Heat Trans. Eng.*, vol. 38, no. 1, pp. 122–136, 2017.

[46] C. Soulaine and M. Quintard, "On the use of Darcy-Forchheimer like model for a macro-scale description of turbulence in porous media and its application to structured packings," *Int. J. Heat Mass Trans.*, vol. 74, pp. 88–100, 2014.
[47] Y. Jin, M.-F. Uth, A. Kuznetsov, and H. Herwig, "Numerical investigation of the possibility of macroscopic turbulence in porous media: A direct numerical simulation study," *J. Fluid Mech.*, vol. 766, pp. 76–103, 2015.
[48] M. Chandesris, A. D'Hueppe, B. Mathieu, D. Jamet, and B. Goyeau, "Direct numerical simulation of turbulent heat transfer in a fluid-porous domain," *Phys. Fluids*, vol. 25, no. 12, pp. 125110, 2013.
[49] M. Agnaou, D. Lasseux, and A. Ahmadi, "From steady to unsteady laminar flow in model porous structures: An investigation of the first Hopf bifurcation," *Comput. Fluids*, vol. 136, pp. 67–82, 2016.
[50] M. de Lemos, *Turbulence in Porous Media: Modeling and Applications*. London, UK: Elsevier Science Ltd, 2006.
[51] B. Antohe and J. Lage, "A general two-equation macroscopic turbulence model for incompressible flow in porous media," *Int. J. Heat Mass Trans.*, vol. 40, no. 13, pp. 3013–3024, 1997.
[52] D. Getachew, W. Minkowycz, and J. Lage, "A modified form of the κ–ε model for turbulent flows of an incompressible fluid in porous media," *Int. J. Heat Mass Trans.*, vol. 43, no. 16, pp. 2909–2915, 2000.
[53] F. Kuwahara, Y. Kameyama, S. Yamashita, and A. Nakayama, "Numerical model of turbulent flow in porous media using a spatially periodic array," *J. Porous Media*, vol. 1, pp. 47–55, 1998.
[54] A. Nakayama and F. Kuwahara, "A macroscopic turbulence model for flow in a porous medium," *J. Fluids Eng.*, vol. 121, no. 2, pp. 427–433, 1999.
[55] M. H. Pedras and M. J. de Lemos, "Macroscopic turbulence modeling for incompressible flow through undeformable porous media," *Int. J. Heat Mass Trans.*, vol. 44, no. 6, pp. 1081–1093, 2001.
[56] Y. Achdou, O. Pironneau, and F. Valentin, "Effective boundary conditions for laminar flows over periodic rough boundaries," *J. Comput. Phys.*, vol. 147, pp. 187–218, 1998.
[57] S. Veran, Y. Aspa, and M. Quintard, "Effective boundary conditions for rough reactive walls in laminar boundary layers," *Int. J. Heat Mass Trans.*, vol. 52, pp. 3712–3725, 2009.
[58] C. Introïni, M. Quintard, and F. Duval, "Effective surface modeling for momentum and heat transfer over rough surfaces: Application to a natural convection problem," *Int. J. Heat Mass Trans.*, vol. 54, pp. 3622–3641, 2011.
[59] R. Lenormand, E. Touboul, and C. Zarcone, "Numerical models and experiments on immiscible displacements in porous media," *J. Fluid Mech.*, vol. 189, pp. 165–187, 1988.
[60] B. Zhao, C. MacMinn, and R. Juanes, "Wettability control on multiphase flow in patterned microfluidics," *Proc. Natl. Acad. Sci. USA*, vol. 111, no. 37, pp. 10251–10256, 2016.
[61] W. B. Haines, "Studies in the physical properties of soil. v. the hysteresis effect in capillary properties, and the modes of moisture distribution associated therewith," *J. Agric. Sci.*, vol. 20, no. 1, pp. 97–116, 1930.
[62] S. Berg et al., "Real-Time 3D imaging of Haines jumps in porous media flow," *Proc. Natl. Acad. Sci.*, vol. 110, no. 10, pp. 3755–3759, 2013.
[63] T. Ransohoff, P. Gauglitz, and C. Radke, "Snap-Off of gas bubbles in smoothly constricted noncircular capillaries," *AIChE J.*, vol. 33, no. 5, pp. 753–765, 1987.
[64] A. Kovscek and C. Radke, "Gas bubble Snap-Off under Pressure-Driven flow in constricted noncircular capillaries," *Colloids Surf. A: Physicochem. Eng. Aspects*, vol. 117, no. 1, pp. 55–76, 1996.
[65] B. Legait, "Laminar flow of two phases through a capillary tube with variable square cross-section," *J. Colloid Interf. Sci.*, vol. 96, no. 1, pp. 28–38, 1983.
[66] I. Chatzis, N. R. Morrow, and H. T. Lim, "Magnitude and detailed structure of residual oil saturation," *Soc. Petrol. Eng. J.*, vol. 23, no. 2, pp. 311–326, 1983.
[67] S. Schlüter, S. Berg, M. Rücker, R. Armstrong, H.-J. Vogel, R. Hilfer, and D. Wildenschild, "Pore-scale displacement mechanisms as a source of hysteresis for two-phase flow in porous media," *Water Resour. Res.*, vol. 52, no. 3, pp. 2194–2205, 2016.
[68] N. R. Morrow and C. C. Harris, "Capillary equilibrium in porous materials," *Soc. Petrol. Eng. J.*, vol. 5, no. 1, pp. 15–24, 1965.
[69] F. Kalaydjian, "A macroscopic description of multiphase flow in porous media involving spacetime evolution of fluid/fluid interface," *Transp. Porous Media*, vol. 2, no. 6, pp. 537–552, 1987.
[70] W. G. Gray and S. M. Hassanizadeh, "Unsaturated flow theory including interfacial phenomena," *Water Resour. Res.*, vol. 27, no. 8, pp. 1855–1863, 1991.
[71] M. Hassanizadeh and W. G. Gray, "Toward an improved description of the physics of two-phase flow," *Adv. Water Resour.*, vol. 16, no. 1, pp. 53–67, 1993.
[72] P. C. Reeves and M. A. Celia, "A functional relationship between capillary pressure, saturation, and interfacial area as revealed by a pore-scale network model," *Water Resour. Res.*, vol. 32, no. 8, pp. 2345–2358, 1996.
[73] F. Dullien, *Porous Media: Fluid Transport and Pore Structure*. New York, USA: Academic Press, 1979.
[74] R. Lenormand, "Liquids in Porous Media," *J. Phys.: Cond. Matter*, vol. 2, no. S, pp. SA79–SA88, 1990.
[75] J.-L. Auriault, "Nonsaturated deformable porous media: Quasistatics," *Transp. Porous Media*, vol. 2, pp. 45–64, 1987.
[76] W. Rose, "Measuring transport coefficients necessary for the description of coupled two-phase flow of immiscible fluids in porous media," *Transp. Porous Media*, vol. 3, pp. 163–171, 1988.
[77] F. Kalaydjian, "Origin and quantification of coupling between relative permeabilities for two-phase flows in porous media," *Transp. Porous Media*, vol. 5, pp. 215–229, 1990.
[78] D. Lasseux, M. Quintard, and S. Whitaker, "Determination of permeability tensors for two-phase flow in homogeneous porous media: Theory," *Transp. Porous Media*, vol. 24, pp. 107–137, 1996.
[79] B. J. Bourbiaux and F. J. Kalaydjian, "Experimental study of cocurrent and countercurrent flows in natural porous media," *SPE Reservoir Eng.*, vol. 5, pp. 361–368, 1990.
[80] C. Zarcone and R. Lenormand, "Détermination Expérimentale du couplage visqueux dans les Écoulements

diphasiques en milieu poreux," *C. R. Acad. Sci. Paris II*, vol. 318, pp. 1429–1435, 1994.
[81] W. Rose, "Myths about Later-Day extensions of Darcy's law," *J. Petrol. Sci. Eng.*, vol. 26, no. 1–4, pp. 187–198, 2000.
[82] J. C. Bacri, M. Chaouche, and D. Salin, "Modèle simple de Perméabilités relatives Croisées," *C. R. Acad. Sci. Paris II*, vol. 311, pp. 591–597, 1990.
[83] R. Clavier, N. Chikhi, F. Fichot, and M. Quintard, "Modeling of inertial multi-phase flows through high permeability porous media: Friction closure laws," *Int. J. Multiph. Flow*, vol. 91, pp. 243–261, 2017.
[84] V. Dhir and L. Barleon, "Dryout heat-flux in a bottom-heated porous layer," *Trans. Amer. Nucl. Soc.*, vol. 38, pp. 385–386, 1981.
[85] R. J. Lipinski, "Model for boiling and dryout in particle beds. [LMFBR]," Sandia National Labs., Albuquerque, NM (USA),Technical Rep. NUREG/CR-2646, 1982.
[86] T. Schulenberg and U. Müller, "An improved model for two-phase flow through beds of coarse particles," *Int. J. Multiph. Flow*, vol. 13, pp. 87–97, 1987.
[87] N. Chikhi, R. Clavier, J.-P. Laurent, F. Fichot, and M. Quintard, "Pressure drop and average void fraction measurements for two-phase flow through highly permeable porous media," *Annal. Nuclear Energy*, vol. 94, pp. 422–432, 2016.
[88] C. L. Hearn, "Simulation of stratified waterflooding by pseudo relative permeability curves," Paper SPE 2929 presented at the 45th Annual Fall Meeting of the Society of Petroleum Engineers, Houston, October 4, 1970.
[89] J. R. Kyte et al., "New pseudo functions to control numerical dispersion," *Soc. Petrol. Eng. J.*, vol. 15, no. 4, pp. 269–276, 1975.
[90] J. Barker and S. Thibeau, "A critical review of the use of pseudorelative permeabilities for upscaling," *SPE Reservoir Eng.*, vol. 12, pp. 138–143, 1997.
[91] M. Quintard and S. Whitaker, "Fundamentals of transport equation formulation for two-phase flow in homogeneous and heterogeneous porous media," in *Vadose Zone Hydrology: Cutting Across Disciplines*, M. B. Parlange and J. W. Hopmans, eds. New York: Oxford University Press, 1999, pp. 3–57.
[92] A. Hashemi and S. R. Shadizadeh, "The impact of reservoir properties on pseudo functions: Upscaling of relative permeability," *Petrol. Sci. Technol.*, vol. 32, no. 7, pp. 772–782, 2014.
[93] M. Quintard and S. Whitaker, "Two-Phase flow in heterogeneous porous media I: The influence of large spatial and temporal gradients," *Transp. Porous Media*, vol. 5, pp. 341–379, 1990.
[94] R. Hilfer, "Macroscopic equations of motion for two-phase flow in porous media," *Phys. Rev. E*, vol. 58, no. 2, pp. 2090–2096, 1998.
[95] M. Panfilov and I. Panfilova, "Phenomenological meniscus model for two-phase flows in porous media," *Transp. Porous Media*, vol. 58, no. 1–2, pp. 87–119, 2005.
[96] L. Cueto-Felgueroso and R. Juanes, "A phase field model of unsaturated flow," *Water Resour. Res.*, vol. 45, no. 10, pp. 1–23, 2009.
[97] J. Buchlin and A. Stubos, "Phase change phenomena at liquid saturated self heated particulate beds," in *Modelling and Applications of Transport Phenomena in Porous Media*, J. Bear. and J. M. Buchlin, eds. Dordrecht, The Netherlands: Springer, 1991, pp. 221–276.
[98] M. Fourar, R. Lenormand, and F. Larachi, "Extending the F-function concept to Two-Phase flow in trickle beds," *Chem. Eng. Sci.*, vol. 56, pp. 5987–5994, 2001.
[99] A. Reed, "The effect of channeling on the dryout of heated particulate beds immersed in a liquid pool," Ph.D. dissertation, Massachusetts Institute of Technology, Cambridge, Massachusetts, USA, 1982.
[100] R. J. Lipinski, "A coolability model for post accident nuclear reactor debris," *Nucl. Technol.*, vol. 65, pp. 53, 1984.
[101] K. Hu and T. Theofanous, "On the measurement and mechanism of dryout in volumetrically heated coarse particle beds," *Int. J. Multiph. Flow*, vol. 17, pp. 519–532, 1991.
[102] D. Lasseux, A. Ahmadi, and A. Arani, "Two-phase inertial flow in homogeneous porous media: A theoretical derivation of a macroscopic model," *Transp. Porous Media*, vol. 75, pp. 371–400, 2008.
[103] N. Tutu, T. Ginsberg, J. Klein, J. Klages, and C. Schwarz, "Debris bed quenching under bottom flood conditions (in-vessel degraded core cooling phenomenology) [PWR]," Brookhaven National Lab., Upton, Suffolk County, New York, USA, Technical Rep. NUREG/CR-3850, 1984.
[104] R. Clavier, N. Chikhi, F. Fichot, and M. Quintard, "Two-phase flow in porous media at high Reynolds number: Discussion of macro-scale models based on new experimental data," Paper A0207, ISHT-9, Beijing, China, Aug. 15–19, 2016.
[105] R. J. Lipinski, "A one-dimensional particle bed dryout model," *Trans. Amer. Nucl. Soc.*, vol. 38, pp. 386–387, 1981.
[106] A.-W. Reed, E.-D. Bergeron, K.-R. Boldt, and T.-R. Schmidt, "Coolability of UO_2 debris beds in pressurized water pools: DCC-1 & DCC-2 experiment results," *Nucl. Eng. Des.*, vol. 97, pp. 81–88, 1986.
[107] V. Tung and V. Dhir, "A hydrodynamic model for two-phase flow through porous media," *Int. J. Multiph. Flow*, vol. 14, pp. 47–65, 1988.
[108] V. Tung and V. Dhir, "On fluidization of a particulate bed during quenching by flooding from the bottom," Proceedings of the 6th Information Exchange Meeting on Debris Bed coolability, Los Angeles, CA, USA, Nov. 7–9, 1984, pp. 14–1–14–13, 1986.
[109] M. Taherzadeh and M. Saidi, "Modeling of two-phase flow in porous media with heat generation," *Int. J. Multiph. Flow*, vol. 69, pp. 115–127, 2015.
[110] B. Mahr and D. Mewes, "CFD modelling and calculation of dynamic two-phase flow in columns equipped with structured packing," *Chem. Eng. Res. Des.*, vol. 85, no. 8, pp. 1112–1122, 2007.
[111] B. Mahr and D. Mewes, "Two-phase flow in structured packings: Modeling and calculation on a macroscopic scale," *AIChE J.*, vol. 54, no. 3, pp. 614–626, 2008.
[112] C. Soulaine, Y. Davit, and M. Quintard, "A two-pressure model for slightly compressible single phase flow in bi-structured porous media," *Chem. Eng. Sci.*, vol. 96, pp. 55–70, 2013.

[113] C. Soulaine, P. Horgue, J. Franc, and M. Quintard, "Gas–liquid flow modeling in columns equipped with structured packing," *AIChE J.*, vol. 60, no. 10, pp. 3665–3674, 2014.
[114] M. Fourati, V. Roig, and L. Raynal, "Liquid dispersion in packed columns: Experiments and numerical modeling," *Chem. Eng. Sci.*, vol. 100, pp. 266–278, 2013.
[115] C. Soulaine, "Modélisation des Écoulements dans les garnissages structurés: de l'Échelle du pore à l'Échelle de la colonne," Ph.D. dissertation, University of Toulouse, Toulouse, France, 2012.
[116] F. Augier, A. Koudil, A. Royon-Lebeaud, L. Muszynski, and Q. Yanouri, "Numerical approach to predict wetting and catalyst efficiencies inside trickle bed reactors," *Chem. Eng. Sci.*, vol. 65, no. 1, pp. 255–260, 2010.
[117] J.-C. Charpentier and M. Favier, "Some liquid holdup experimental data in trickle-bed reactors for foaming and nonfoaming hydrocarbons," *AIChE J.*, vol. 21, no. 6, pp. 1213–1218, 1975.
[118] K. Ng and C. Chu, "Trickle-bed reactors," *Chem. Eng. Progr.*, vol. 83, no. 11, 1987.
[119] M. Kondo and K.-I. Nakajima, "Experimental investigation of air-water two phase upflow across horizontal tube bundles: Part 1, flow pattern and void fraction," *Bull. Japan Soc. Mech. Eng.*, vol. 23, no. 177, pp. 385–393, 1980.
[120] T. R. Melli, J. M. De Santos, W. B. Kolb, and L. Scriven, "Cocurrent downflow in networks of passages. Microscale roots of macroscale flow regimes," *Ind. Eng. Chem. Res.*, vol. 29, no. 12, pp. 2367–2379, 1990.
[121] P. Horgue, F. Augier, P. Duru, M. Prat, and M. Quintard, "Experimental and numerical study of two-phase flows in arrays of cylinders," *Chem. Eng. Sci.*, vol. 102, pp. 335–345, 2013.
[122] L. Raynal, F. Augier, F. Bazer-Bachi, Y. Haroun, and C. P. da Fonte, "CFD applied to process development in the oil and gas industry–A review," *Oil Gas Sci. Technol.*, vol. 71, no. 3, pp. 42, 2015.
[123] M. Sahimi, *Applications of Percolation Theory*. London, UK: CRC Press, 1994.
[124] T. R. Melli and L. Scriven, "Theory of two-phase cocurrent downflow in networks of passages," *Ind. Eng. Chem. Res.*, vol. 30, no. 5, pp. 951–969, 1991.
[125] V. Joekar-Niasar and S. Hassanizadeh, "Analysis of fundamentals of two-phase flow in porous media using dynamic pore-network models: A review," *Crit. Rev. Environ. Sci. Technol.*, vol. 42, no. 18, pp. 1895–1976, 2012.
[126] R. Hannaoui, P. Horgue, F. Larachi, Y. Haroun, F. Augier, M. Quintard, and M. Prat, "Pore-network modeling of trickle bed reactors: Pressure drop analysis," *Chem. Eng. J.*, vol. 262, pp. 334–343, 2015.
[127] R. Guibert, P. Horgue, G. Debenest, and M. Quintard, "A comparison of various methods for the numerical evaluation of porous media permeability tensors from Pore-Scale geometry," *Math. Geosci.*, vol. 48, no. 3, pp. 329–347, 2016.

Appendix: Closure problem for Darcy's law

There are several possible versions of the closure problems. The one corresponding to the mapping given by Eqs. (16) is described by the following PDEs

$$\nabla.\mathbf{B} = 0 \tag{A1}$$

$$-\nabla\mathbf{b} + \nabla^2\mathbf{B} = \varepsilon_\beta^{-1}\frac{1}{V}\int_{A_{\beta\sigma}} \mathbf{n}_{\beta\sigma}\,.\,(-\mathbf{I}\mathbf{b} + \nabla\mathbf{B})\; dA \tag{A2}$$

$$\mathbf{B} = -\mathbf{I} \quad \text{at } A_{\beta\sigma} \tag{A3}$$

$$\langle\mathbf{b}\rangle^\beta = 0 \tag{A4}$$

$$\mathbf{b}(\mathbf{r}+\mathbf{l}_i) = \mathbf{b}(\mathbf{r}) \qquad \mathbf{B}(\mathbf{r}+\mathbf{l}_i) = \mathbf{B}(\mathbf{r}). \tag{A5}$$

The mapping tensor $\mathbf{B}$ has the following property

$$\langle\mathbf{B}\rangle^\beta = 0 \tag{A6}$$

which, together with Eq. (A4), ensure that the averages of the deviations are zero.

Other forms can be developed to eliminate the integro-differential terms in the closure problem, see [78] for such transformations. This generally leads to problems that are similar to a Stokes problem over a periodic unit cell with a constant source term (the gradient of the averaged pressure). Such a form can readily be used to calculate the permeability tensor from a classical CFD software. The use of periodicity conditions is correct for periodic systems. This approximation, however, may pose problems for systems which are not truly periodic. This point is not discussed further in this paper and the reader may look at the literature on the subject, for instance, in [127], for indications on how to overcome this difficulty.